Engineering metabolic time-sharing in a clonal *Escherichia coli* population

Fotini Papazotos

A thesis
in
the Department
of
Biology

Presented in Partial Fulfillment of the Requirements
for the Degree of Master of Science (Biology) at
Concordia University
Montréal Québec, Canada

May 2023

CONCORDIA UNIVERSITY
School of Graduate Studies

This is to certify that the thesis prepared

By: Fotini Papazotos

Entitled: Engineering metabolic time-sharing in a clonal *Escherichia coli* population

and submitted in partial fulfillment of the requirements for the degree of

Master of Science (Biology)

complies with the regulations of the University and meets the accepted standards with respect to originality and quality.

Signed by the final examining committee:

Dr. David Walsh Chair

Dr. Vincent Martin Examiner

Dr. Isabelle Benoit-Gelber Examiner

Dr. Laurent Potvin-Trottier Thesis Supervisor(s)

Thesis Supervisor(s)

Approved by Dr. Grant Brown
Chair of Department or Graduate Program Director

Dr. Pascale Sicotte Dean of Arts & Science

ABSTRACT

Engineering metabolic time-sharing in a clonal *E. coli* population

Fotini Papazotos

The "division of labour" strategy is common among microbial communities, as dividing burdensome tasks between members of a community alleviates the strain placed on individual cells. Exploiting this phenomenon in heterogeneous microbial co-cultures for industrial synthesis of valuable compounds is limited by inefficiencies in nutrient exchange and conflicting growth requirements. Here, we demonstrate a synthetic gene circuit which enables cells of an isogenic *Escherichia coli* population to carry out "metabolic time-sharing" by shifting between alternate metabolic states via temporal changes in gene expression. Further, we review techniques for monitoring such dynamic processes at the single-cell level, and discuss their current applications in bacterial studies. To validate that our circuit may be used to induce cooperative behaviours in microbial populations, we adapted this circuit to engineer cells that oscillate between distinct amino acid auxotrophy phenotypes, driven by the periodic silencing of key biosynthetic genes. Culturing a clonal time-sharing population with unsynchronized oscillators permits reciprocal amino acid cross-feeding, ultimately ensuring population viability. Through comparative growth experiments, we found that the fitness of our time-sharing population was comparable to that of a heterogeneous co-culture composed of *E. coli* auxotrophs similarly capable of cross-feeding amino acids. Although future studies would be needed to confirm this, our preliminary results suggest that metabolic time-sharing may be a viable alternative to synthetic heterogeneous co-cultures. As it may enable an entire complex biosynthetic pathway to be engineered into a single host with reduced metabolic burden, the metabolic time-sharing strategy demonstrated here could potentially be implemented for microbial bioproduction, among other widespread applications.

ACKNOWLEDGEMENTS

This work was only made possible by the overwhelming support that I have received from many people. First, I would like to thank Dr. Laurent Potvin-Trottier for his mentorship and guidance, and for believing in me as a scientist. It has been a pleasure working in the lab these past few years. I would also like to thank my committee members, Dr. Vincent Martin and Dr. David Walsh for their valuable feedback regarding this project.

I want to think my amazing labmates for the many dumpling lunches, days spent in the park, and for putting up with me when I've been overcaffeinated and underslept. Thank you to Ellie for the help and guidance, and to Saba for always being there to chat or seek out all of the free food on campus. To Paige and Krista, for the equally memorable long days in the lab and evenings spent with pizza and reality TV. Special thanks to Felipe, Maria, Jyler, Maude, and Pierre, for bringing an encouraging and supportive environment to the lab.

This work would not have been possible without funding from the NSERC-CGS-M and FRQNT Doctoral scholarships, as well as the SynBioApps NSERC CREATE and Miriam Aaron Roland fellowships.

I would also like to thank my parents Liz and George and my brother Jimmy for providing support and encouragement throughout my (many) years of study. Lastly, I want to thank my partner Mario for listening to me talk endlessly about bacteria, and for the steady support through the final stages of this thesis.

This thesis is dedicated to my cat, Feta, who has been a source of joy and comfort through the ups and downs of grad school, and who provided valuable insight into this thesis by meowing all day while I was writing.

AUTHOR CONTRIBUTIONS

The thesis project was conceived by Dr. Laurent Potvin-Trottier. Giselle McCallum provided scripts for analyzing microbial growth data. All plasmids and strains were created by Fotini Papazotos, with the exception of gifts (referenced in Chapter 5). All experiments were designed, performed, and analyzed by Fotini Papazotos. Figures were created in part using BioRender.

Chapter 2 is a review article published in *Frontiers in Bioengineering and Biotechnology* (2022), co-first authored by Fotini Papazotos and Paige Allard, alongside Dr. Laurent Potvin-Trottier. Fotini Papazotos and Paige Allard contributed equally to this manuscript. Additionally, Krista Jager helped create the figures for this review, and Giselle McCallum, Felipe Perez, Maria Orozco-Hidalgo, and Krista Jager provided comments and feedback about the manuscript. This review provides background information and motivation for the use of single-cell techniques within this thesis:

Paige Allard[†], Fotini Papazotos[†], & Laurent Potvin-Trottier. Microfluidics for long-term single-cell time-lapse microscopy: Advances and Applications. *Front Bioeng. Biotechnol.* **12**, 1881 (2022).

[†]These authors contributed equally to this work

TABLE OF CONTENTS

LIST OF FIGURES

LIST OF TABLES

CHAPTER 1

INTRODUCTION

1.1 Interactions in microbial communities

Microbes, which cumulatively make up approximately 13% of the biomass on Earth[1], generally exist in diverse and heterogeneous communities. Interactions between microbes in a mixed environment may be neutral, or they may impact the fitness of their participants in a positive or negative manner[2–5]. For example, microbial species within complex communities may behave antagonistically and impede the survival of competitors either directly, via release of antibiotics or other toxins into the environment[6–9], or indirectly by outcompeting others in acquiring limited nutrients[8,10,11] (Fig 1.1). Conversely, communities may exhibit beneficial interactions which incur positive fitness consequences for those involved. Commensalism represents one type of uni-directional beneficial interaction, in which one member receives a fitness benefit from their partner, whose own fitness remains unaffected[12] (Fig 1.1). Consuming excreted metabolic by-products is one example of commensalism, as the fitness of the producing species remains unaltered, while proximal interactors reap the benefits of consuming these readily available nutrients[12].

Beneficial interactions can also be bi-directional, such that all participants in the interaction behave cooperatively and receive a fitness benefit. This type of behaviour is exemplified in "cross-feeding" interactions, wherein individuals with distinct but complementary metabolic capabilities reciprocally share nutrients that their interacting partner lacks the capacity to produce[4,13–16] (Fig 1.1). Cross-feeding enables "division of labour" (DOL)[17–21] between members of microbial consortia, as metabolic specialization facilitates the efficient allocation of tasks to specialized individuals. However, these interactions have the potential to be exploited by non-cooperating or "cheating" individuals, which have access (and therefore opportunity) to consume these shared nutrients without the burden of providing any in return[18,22,23] (Fig 1.1). Gaining a deep understanding of these natural, complex community dynamics can enable the engineering of synthetic systems exhibiting similar behaviours.

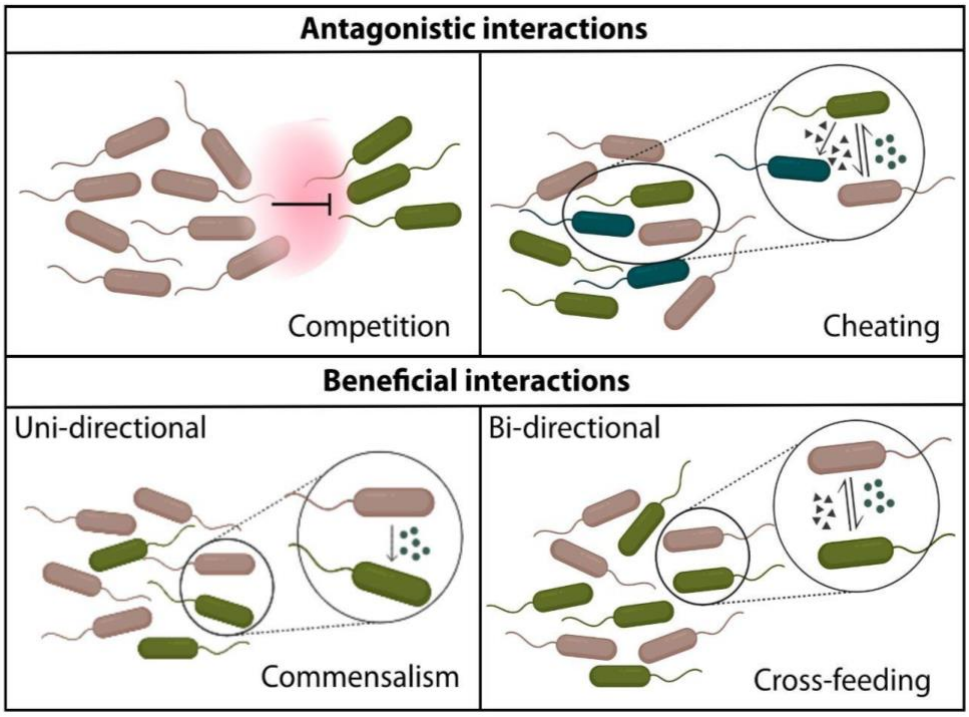

Figure 1.1 Types of community interactions. Members of a microbial community may exhibit antagonistic behaviour through competition for limited resources or siphoning of nutrients produced by individuals engaged in beneficial reciprocal relationships ("cheating"). Such interactions threaten to destabilize the community, as they solely promote the survival of the individuals engaging in antagonistic behaviour. Conversely, communities may engage in mutually beneficial interactions that maintain community stability. These may be uni-directional, providing a fitness advantage to one partner while having no effect on the fitness of the other, as is the case for commensalism. In the case of bi-directional beneficial interactions such as reciprocal cross-feeding, all members involved receive a fitness benefit from the interaction, thereby reinforcing community stability.

1.2 Division of labour in microbial consortia

DOL refers to the delegation of tasks between cooperating individuals to reach a shared goal[21], and has been widely utilized by a variety of biological systems. This strategy is exemplified in the colony organization of social insects such as ants or honeybees, as division of worker and queen castes determines an individual's specialized role in the community[24,25]. In multicellular organisms, DOL is exerted through differentiation of specialized cell types which each carry out

distinct functional roles to ensure survival of the organism[26,27]. DOL enables specialization by splitting the burden of carrying out essential tasks between distinct, cooperating individuals.

In natural microbial communities, DOL has been employed as a strategy to carry out complex metabolic pathways. The nitrification pathway represents one such example, as the oxidation of ammonia into nitrite and subsequent oxidation of nitrite into nitrate are each carried out by distinct groups of bacteria[28,29]. Ultimate production of biologically available nitrate therefore relies on both groups carrying out these complementary metabolic processes[28]. Similarly, the synergistic conversion of syringic acid to acetate has been observed in a co-culture of *Acetobacterium woodii* and *Pelobacter acidigallici*, with neither species exhibiting the capacity to carry out this conversion in isolation[30].

The utilitization of DOL in natural communities has prompted the engineering of synthetic microbial consortia for coordinated and synergistic completion of tasks with widespread applications[15,23,31]. As interest in renewable energy sources has been growing in recent years, so has the development of microbial co-cultures for processing complex precursors such as lignocellulosic biomass into biofuels[32–35]. The synthesis of ethanol and diesel from carbohydrates has been demonstrated in engineered hosts such as *Escherichia coli*[36,37] and *Saccharomyces cerevisiae*[38]. However, attempts at consolidating all necessary steps into a single strain through co-expression of multiple heterologous enzymes have thus far limited product titers[39]. To address this constraint, dividing the tasks of lignocellulose hydrolysis and biofuel synthesis into separate species has enabled successful, albeit inefficient, biofuel production[40,41].

Alternatively, DOL has been implemented into synthetic microbial consortia as a means of improving community fitness. This was demonstrated in co-cultures wherein each member is auxotrophic for one amino acid, but simultaneously overproduces another to complement its partner's auxotrophy[15,31,42]. Reciprocal cross-feeding of these desired amino acids relieves each individual of the metabolic burden of producing one amino acid, which it is instead able to obtain from interacting partners. Interestingly, one study investigating different amino acid cross-feeding pairs found that the overall fitness of these co-cultures were elevated by up to 20% compared to a prototrophic monoculture[15]. DOL can thus be incorporated in the design of cooperative microbial

consortia as a means of increasing productivity and fitness, with applications in the biotechnology industry for efficient biosynthesis of valuable products.

1.3 Employment of microbial hosts in the biotechnology industry

In recent years, microbial hosts have been increasingly employed for the production of valuable products and biologics as an alternative to chemical synthesis[43,44]. As well-characterized organisms for which numerous genetic engineering tools have been developed, *E. coli, S. cerevisiae,* and *Pichia pastoris* have been widely used as microbial bioproduction hosts (Fig 1.2A). However, despite its utility and versatility, several factors limit the efficiency and ultimate product yield that may be obtained using microbial hosts for industrial fermentation.

The expression of complex heterologous pathways and redirection of metabolic flux toward product synthesis can create strain on limited pools of cellular resources[19]. This burden may result in slower host growth rates[19,45] and bioproduction rates below the theoretical maximum yield[46,47]. Therefore, DOL strategies have been applied to microbial bioproduction as a means of distributing this burden between multiple hosts.

1.3.1 Application of DOL strategies for enhanced microbial bioproduction

Efforts to maximize the efficiency of microbial fermentation processes have implemented DOL strategies through the use of microbial co-cultures[44,47–51]. To reduce metabolic burden, a biosynthetic pathway responsible for product synthesis is divided into distinct stages, or "modules", with each member of a multi-strain or multi-species consortia being tasked with the expression of one module[44,47–49,51–53] (Fig 1.2B). In a co-culture environment, an intermediate molecule produced via the activity of one module may then be shared with other members of the consortia to drive flux through subsequent pathway modules. This cross-feeding of pathway intermediates could enable the coordinated synthesis of the desired compound by the microbial consortia, while reducing the metabolic strain placed on each individual.

The co-culture strategy has been used for the successful production of a variety of compounds, including biofuels[40], dyes[51], and precursor molecules for the synthesis of pharmaceuticals[49] and polyurethanes[47,48]. Current methods for chemically synthesizing these compounds may be costly, resource-intensive, and unsustainable, indicating a need for microbial fermentation methods lacking these drawbacks. For example, traditional methods of synthesizing the polyurethane precursor, adipic acid, relies on nonrenewable petroleum feedstocks and releases the greenhouse gas nitrous oxide during the process[54]. Alternatively, adipic acid can be synthesized by hydrogenating its precursor, muconic acid[54]. Sustainable muconic acid biosynthesis has been demonstrated by *E. coli* consortia fed on renewable carbon sources such as glycerol, with each member of the two-strain co-culture engineered to efficiently express one pathway module[47]. Ultimate product synthesis was facilitated by cross-feeding of the intermediate molecule 3-dehydroshikimic acid (DHS) between individuals expressing different modules. Adopting a DOL strategy vastly improved production, as the cooperative *E. coli* co-culture was able to produce 1016 mg/L muconic acid, while a single host strain engineered to express the entire synthesis pathway produced only 56 mg/L[47]. This dramatic increase in product synthesis highlights the benefits of implementing DOL into microbial bioproduction strategies.

Although the use of microbial co-cultures for compound synthesis appears promising, there are disadvantages that may limit overall product yield. Primarily, culturing multiple hosts together within the same bioreactor environment can yield unstable community dynamics[23,47,48]. Competition for shared nutrients, or differences in growth rates and nutrient requirements between hosts may result in one strain dominating the community. An imbalance in host abundances can hinder progression through the shared pathway, thus decreasing product yield. Additionally, the loss of intermediate molecules through incomplete transfer between hosts prevents a co-culture from reaching the theoretical maximum yield of the desired product[23]. These limitations, which are inherent to heterogeneous microbial consortia, illustrate the demand for a single-strain microbial fermentation system capable of exhibiting DOL.

1.4 Dynamic cellular processes

A number of natural microbial populations have been shown to alter the dynamics of their cellular processes to coordinate DOL. A notable example of this is the ability of natural *Bacillus subtilis* populations to use an innovative "molecular time-sharing" strategy to address competition between alternative sigma factors for limited RNA polymerase binding opportunities[55]. Rather than assuming the burden associated with increasing RNA polymerase expression, each cell alternates between RNA polymerase binding to different sigma factors over time[55]. The dynamic changes in gene expression profiles that result from transcription of distinct gene sets by different alternative sigma factors may function to ensure overall population survival in the face of different environmental stressors.

Another example of temporal DOL also occurs within natural *B. subtilis* populations. Acetate is produced as a by-product of cellular metabolism, and its resultant accumulation creates toxic conditions for *B. subtilis* by lowering intracellular pH[56]. To combat this, a fraction of the isogenic population stochastically switches into a distinct metabolic state which instead produces the pH-neutral molecule acetoin[56]. Uptake of excreted acetoin maintains population viability by neutralizing the acidic pH created as a result of acetate accumulation. Although the production of acetoin imposes an increased metabolic burden on this subpopulation, such division of metabolic labour was hypothesized to improve overall population fitness. The stochastic switching between distinct states may act as a means for isogenic populations to carry out necessary but opposing metabolic tasks.

Similarly, cyanobacteria have been shown to coordinate dynamic changes in gene expression in order to carry out essential, but incompatible metabolic functions. Cyanobacteria carry out both photosynthesis and nitrogen fixation, despite the incompatibility of these processes due to the irreversible inactivation of the nitrogenase enzyme by oxygen[21,22,57]. Some non-heterocystous groups including the *Oscillatoria* species have adopted a method for temporally dividing these tasks. These species of cyanobacteria oscillate between distinct metabolic states in which they perform photosynthesis during the day, and subsequently fix nitrogen at night, according to the dynamics of their circadian rhythm[58–60]. Incorporating temporal, rather than spatial, DOL ensures that all necessary metabolic processes may be executed within the same cell,

thus eliminating the requirement for nutrient transport between cells. While these represent natural examples of dynamic switching between metabolic states, similar behaviour may be implemented into engineered microbial consortia using synthetic gene circuits.

1.4.1 Metabolic time-sharing as a potential solution to decrease host burden

Stochastic fluctuations in gene expression between genetically identical cells can create heterogeneity within a population, resulting in distinct subpopulations exhibiting different phenotypes and behaviours[61–64]. We hypothesize that cells can exhibit "metabolic time-sharing" by alternating between distinct cellular states over time via changes in gene expression[55] (Fig 1.2C). We further hypothesize that this phenomenon may be applied to microbial bioproduction through the engineering of clonal strains that encode an entire biosynthetic pathway, but alter their gene expression dynamics to only express one module at any given time. Shifting between pathway modules serves the purpose of reducing metabolic burden compared to strains expressing all steps simultaneously. Similar to the co-culture approach discussed in Section 1.2.1, metabolic time-sharing enables a population as a whole to use DOL to progress through an entire pathway, but is not subject to the disadvantages associated with heterogeneous co-cultures. Therefore, introducing DOL into a genetically identical population is a promising avenue for enhancing microbial bioproduction, requiring precise control over gene expression dynamics.

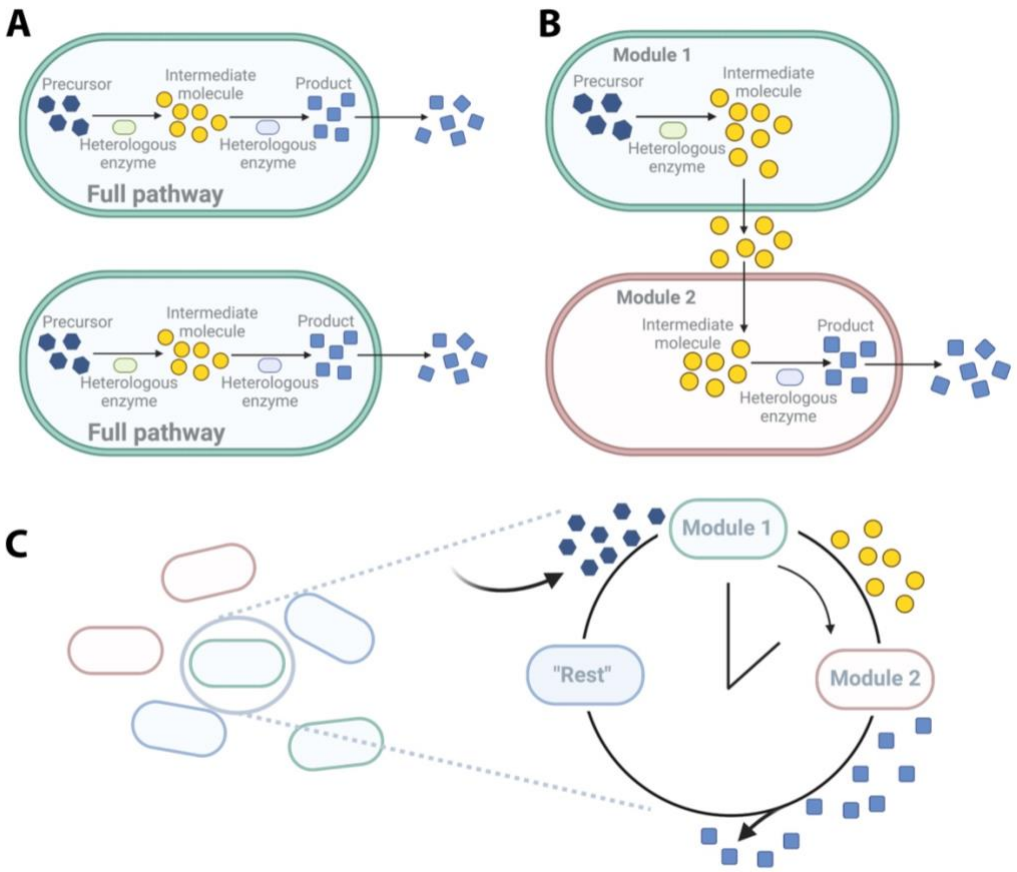

Figure 1.2 Strategies for microbial bioproduction. **(A)** Expressing an entire biosynthetic pathway into an isogenic population, such that each individual has the capacity to produce the desired product. **(B)** Engineering a microbial co-culture, consisting of multiple strains or species that each express one pathway module. Intermediate molecules are shared between members of a heterogeneous community, and overall pathway completion and product synthesis relies on cooperation between cells expressing different modules. **(C)** Implementing metabolic time-sharing in a clonal population enables each member of the population to progress through alternate pathway modules or metabolic states over time. Although the population may appear heterogeneous when metabolic states are unsynchronized between individuals, each cell in the population is genetically identical and capable of independent product synthesis by alternating between distinct states in a specified order.

1.5 Synthetic gene circuits for manipulation of gene expression dynamics

Synthetic gene circuits are networks of genes and regulatory elements designed to dictate host cell behaviour, and may be used to engineer cellular processes with specified dynamics. Parameters including transcription, translation, and depletion rates of regulatory factors such as

repressor proteins, determine the circuit dynamics and may be tuned to achieve the desired temporal behaviour with high precision[65]. The toggle switch represents one classic example of a synthetic circuit that has been used to induce bistable state-switching in cells[66]. This circuit encodes two repressor genes, which each repress the expression of the other to create a bistable system. However, this circuit is limited to two distinct cellular states, and state-switching is not dictated by the circuit itself, but instead must be triggered through inducer molecule addition.

To the contrary, this thesis focuses on the construction and validation of a circuit that enables sustained switching between three distinct cellular states in single *E. coli* cells with specified dynamics, in the absence of inducer molecules. This is achieved by integrating the redesigned repressilator circuit[67], which has been demonstrated to generate precise oscillations in gene expression, with CRISPR interference (CRISPRi)[68], a tool for targeted, transient gene silencing. This hybrid circuit extends the capabilities of the repressilator to enable oscillation of any sets of plasmid- or chromosome-derived genes, and can therefore be used to switch between distinct metabolic states over time through periodic silencing of key metabolic genes. Alternating between complementary metabolic states can facilitate temporal DOL within an isogenic population.

1.5.1 The repressilator

The repressilator is a landmark genetic circuit consisting of three repressor proteins - LacI, TetR and λcI - which each repress the expression of the subsequent repressor in the circuit[67,69]. This creates sustained out-of-phase relaxation oscillations due to delayed negative feedback (Fig 1.3A). Each oscillation begins with a build-up phase characterized by the rapid production of one protein, whose cognate repressor is low in abundance, and ends when production is halted due to the cognate repressor reaching levels sufficient for gene repression (i.e. the "repression threshold"). Cessation of protein production marks the beginning of the decay phase, during which the protein is depleted from the system, enabling de-repression of the subsequent gene in the circuit (Fig 1.3B).

While the original repressilator[69] circuit exhibited noisy behaviour, recent modifications drastically improved its precision[67]. The repressilator circuit used in this thesis lacks degradation tags on the repressor proteins, thereby maintaining high numbers of molecules in the system to

reduce noise caused by stochastic degradation. This ensures that repressor elimination from the system is purely due to dilution, such that the exponential decay phase is intrinsically coupled with cell division. In addition, the repressilator may be used to control the expression of external genes. Placing reporter genes under control of each of the promoters encoded in the circuit (p_{lac}, p_{tet}, and p_R) yields out-of-phase oscillations in reporter gene expression following the same dynamics as the repressilator. However, this circuit is limited to controlling the expression dynamics of external genes placed under the control of p_{lac}, p_{tet}, or p_R, and further development would be required to extend its capabilities to regulate genes controlled by their native promoters.

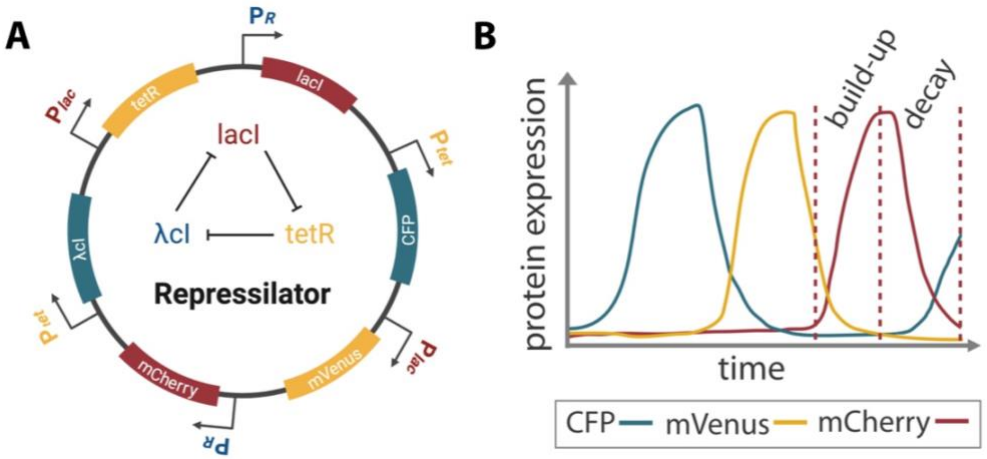

Figure 1.3 Schematic of the repressilator circuit. **(A)** The plasmid-derived repressilator encodes three repressor proteins that each repress the following repressor in the circuit, generating oscillations in repressor gene expression. The "triple-reporter repressilator" variant depicted here additionally encodes three fluorescence genes, each under control of a promoter acted on by the circuit. **(B)** Out-of-phase oscillations generated by the repressilator can be observed by monitoring expression of the three fluorescence genes over time. Schematic representation inspired from Potvin-Trottier *et al*. (2016).

1.5.2 CRISPR interference

CRISPR interference is a versatile tool for specific and transient silencing of target gene expression[68]. Gene silencing requires co-expression of the catalytically dead Cas12 (dCas12) enzyme and a CRISPR array, which encodes alternating "direct repeat" (DR) sequences and "spacers" that are each complementary to a target gene[70,71]. dCas12 facilitates the processing of

CRISPR arrays into mature CRISPR RNA (crRNA) molecules via the trimming of 6-7 base pairs from the 3' end of each spacer, yielding multiple crRNAs encoding single repeat-spacer units[70–72]. Mature crRNA molecules may form complexes with dCas12 enzymes, and guide them to their target genes, thus enabling temporary silencing[71] (Fig 1.4A). CRISPR arrays may encode several crRNAs, which enables flexible, combinatorial gene repression.

Distinct domains of Cas12 exhibit RNase activity for crRNA processing, and DNase activity for target gene cleavage in traditional CRISPR gene editing[71]. However, for transient CRISPRi-mediated gene silencing, a D917A mutation in the DNase domain effectively eliminates DNA cleavage ability[73]. Therefore, when the resultant dCas12 enzyme is guided to its target by a crRNA molecule, it effectively silences transcription of that gene through steric hindrance of RNA polymerase. Although several species have been found to naturally express Cas12, the Cas12 native to *Francisella novicida* has been the most widely used in bacterial genetic engineering applications[72], and the D917A mutant of this homolog is further used throughout this thesis.

While the *Streptococcus pyogenes*-derived dCas9 enzyme has been more widely used in studies implementing CRISPRi[74–78], the more recently discovered dCas12 has proven to be a more versatile alternative. Unlike dCas9[79,80], dCas12 expression has not been reported to cause toxicity in *E. coli* hosts[72], which broadens its potential applications. Additionally, dCas9 does not exhibit crRNA processing capabilities, but instead requires co-expression of an RNase III enzyme to cleave base pairs from the 5' ends of spacers, as well as a trans-activating crRNA (tracrRNA) molecule to facilitate crRNA binding to dCas9[81] (Fig 1.4B). The simplicity of dCas12, which inherently performs the functions of both the RNase III and tracrRNA[71], is advantageous when assembling complex synthetic circuits that additionally require the expression of many different components.

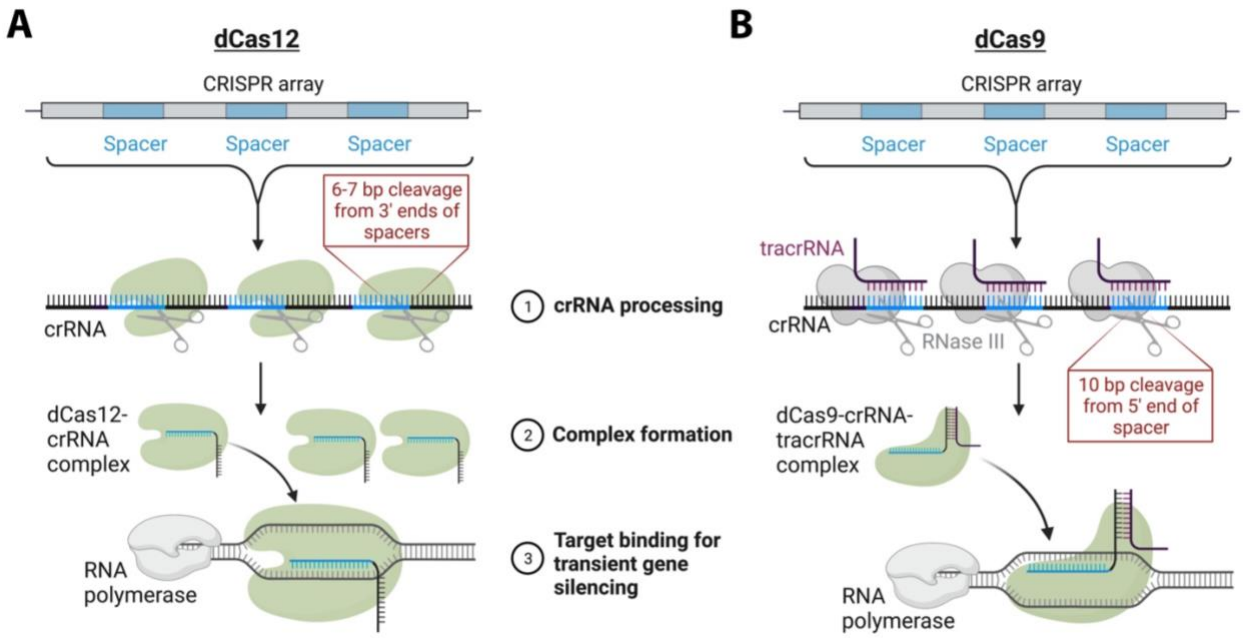

Figure 1.4 Schematic of CRISPR interference. **(A)** In dCas12-mediated CRISPR interference, a CRISPR array is cleaved and processed into discrete crRNAs by dCas12. Each crRNA forms a complex with dCas12, and guides it to a target. Here, the crRNA spacer sequence binds to its complementary target on the noncoding strand, and the associated dCas12 temporarily blocks gene expression by hindering the activity of RNA polymerase. **(B)** As dCas9 does not exhibit crRNA processing ability, RNase III is responsible for CRISPR array cleavage into crRNAs, and a tracrRNA molecule mediates binding of a crRNA molecule to dCas9. The resultant dCas9-crRNA-tracrRNA complex binds to its target on the coding strand and similarly silences gene expression through steric hindrance of RNA polymerase.

1.6 Thesis objectives

In this thesis, we demonstrate a versatile platform for dynamic control over gene expression that can be used to introduce DOL into isogenic bacterial populations. By extending the capabilities of an existing genetic oscillator, we engineer clonal populations that exhibit metabolic time-sharing by alternating between cellular states with predictable dynamics.

Chapter 2 discusses the benefits of monitoring dynamic behaviour at the single-cell level, with emphasis on the "mother machine" microfluidic device, and highlights impactful studies which have employed mother machine-like devices to study dynamic processes in bacteria. In Chapter 3, we present a synthetic gene circuit that dictates oscillations in gene expression and adapt it to construct obligate cross-feeding interactions within clonal *E. coli* populations. To the best of

our knowledge, this is the first instance of exploiting the behaviour of an oscillatory gene circuit to induce cooperative interactions within an isogenic population, and was carried out through two specific aims:

1. Design and construction of a synthetic circuit for dynamic control over gene expression. Here, we integrate the repressilator with CRISPRi to demonstrate a hybrid circuit that oscillates between the expression of alternate CRISPR arrays. We employ a Golden Gate-based method for efficient, modular cloning of CRISPR arrays which dictate cellular states through the targeted, combinatorial repression of metabolic genes.

2. Application of the metabolic time-sharing circuit for the creation of obligate cross-feeding interactions within a clonal E. coli population. In this thesis, we adapt the circuit described in Aim 1 to create an *E. coli* population that alternates between distinct amino acid auxotrophies, thereby enabling reciprocal cross-feeding between proximal cells occupying different states. This proof-of-principle provides evidence that metabolic time-sharing may be used to induce dynamic switching between metabolic states, with potential applications in the biotechnology industry for synthesis of value-added products via successive expression of biosynthetic modules.

CHAPTER 2

MONITORING DYNAMIC PROCESSES

2.1 Introduction

Natural microbial populations have been demonstrated to achieve DOL over time through temporal segregation of complex metabolic processes[55,56,58–60]. The metabolic time-sharing circuit presented here similarly coordinates dynamic switching between cooperative cellular states as a means of increasing the overall fitness of a collaborative population. However, monitoring dynamic cellular processes, whether natural or controlled by engineered synthetic circuits, poses challenges. While kinetic measurements of bulk population behaviour, such as time-lapse growth curves, capture valuable information that is obscured in static "snapshots", these traditional methods that rely on averages may conceal underlying cell-to-cell variability. Techniques capable of tracking single-cells in parallel, including the mother machine microfluidic platform[82], circumvent this limitation and enable the profiling of dynamic phenotypes in heterogeneous populations. Combining population-level and single-cell techniques therefore provides a comprehensive view of population dynamics. In this chapter, we review current single-cell microfluidic technologies and survey their applications in investigating dynamic processes in prokaryotes.

2.2 Abstract

Cells are inherently dynamic, whether they are responding to environmental conditions or simply at equilibrium, with biomolecules constantly being made and destroyed. Due to their small volumes, the chemical reactions inside cells are stochastic, such that genetically identical cells display heterogeneous behaviors and gene expression profiles. Studying these dynamic processes is challenging, but the development of microfluidic methods enabling the tracking of individual prokaryotic cells with microscopy over long time periods under controlled growth conditions has led to many discoveries. This review focuses on the recent developments of one such microfluidic device nicknamed the mother machine. We overview the original device design, experimental setup, and challenges associated with this platform. We then describe recent methods for analyzing experiments using automated image segmentation and tracking. We further discuss modifications

to the experimental setup that allow for time-varying environmental control, replicating batch culture conditions, cell screening based on their dynamic behaviors, and to accommodate a variety of microbial species. Finally, this review highlights the discoveries enabled by this technology in diverse fields, such as cell-size control, genetic mutations, cellular aging, and synthetic biology.

2.3 Background

Genetically identical cells can display strikingly different phenotypes within a fixed environment. In multicellular organisms, this is evident through cell differentiation and specialization. Unicellular organisms can also perform specialized behaviors within a group, such as distinct metabolic states[56] or discrete roles in biofilm formation[83,84]. In addition, some species prepare for changing environmental conditions on a population level by keeping a small fraction of the population ready for such changes, a phenomenon referred to as "bet-hedging"[85,86]. Because biochemical reactions depend on physical interactions between low-abundance molecules, these reactions are inherently stochastic, which results in heterogeneous gene expression between genetically identical cells exposed to the same environment[61–63]. For these reasons, techniques that can measure single-cell properties rather than population averages have revealed important information about many cellular processes, from cell-size control to differentiation. For example, the ability to measure the mRNA profile of single-cells through techniques such as single-cell RNA-seq (scRNAseq) has advanced many fields, as evidenced by the breadth and the number of publications in recent years[87–89]. While such techniques have proven to be very useful, they are typically limited to static snapshots and cannot follow gene expression in individual cells over time. Instead, this is typically achieved using single-cell time-lapse fluorescence microscopy, which for microbes has traditionally involved tracking the growth of single bacteria into microcolonies on agar pads. While technically simple and very useful, agar pads only support growth for a short period of time before cells start competing for nutrients, limiting observation to a few cell divisions[90,91]. Due to limitations in using wide-field fluorescence microscopy (i.e., the point spread function has a long tail), cellular crowding can impact the fluorescence imaging measurements, meaning that the presence of many cells can bias the measured fluorescence of a cell far away[92]. Finally, it can be difficult to change the environmental conditions in this setup, which is important for studying processes such as stress responses. These limitations motivated the development of

microfluidic platforms for single-cell analysis that enables single-cell tracking over many generations under precisely controlled conditions.

The first iterations of microfluidic devices for imaging bacteria utilized closed linear trenches[93] or mono-layer chambers[94] to trap cells. The mono-layer chamber devices[94,95] enable the growth of microcolonies while flushing extra cells and continuously providing growth media, and have been particularly useful for studying group behaviors, such as quorum sensing[96–100]. Continuous culture devices were then developed to enable long-term imaging of bacterial cells undergoing steady-state growth while facilitating the tracking of single cells without crowding limitations, making them ideal for measuring single-cell gene expression[82,91]. A configuration nicknamed the "mother machine" (MM) traps bacteria at the end of single-cell-width dead-end trenches[82]. Newborn cells are flushed out of the device by the constant flow of growth media, thereby allowing single-cell lineages to be followed for hundreds of generations (Fig 2.1). The name "mother machine" refers to the fact that the cells trapped at the end of the trenches are tracked growing and dividing throughout an experiment, and are thus referenced as "mother" cells. A similar layout named the chemostat[91] has trenches open on both sides, thus providing better feeding through convective flow. This device enables long-term time-lapse microscopy while keeping cells that renew both poles and has been used to quantify the maturation time of fluorescent proteins[101].

In this review, we focus on the technical developments of the MM and its applications in the study of bacteria. We start by describing the original design and the constraints that motivated further technical developments. We then overview recent image analysis tools that enable segmentation and tracking of cells in the device using phase contrast images, and modifications to the device that enables the precise control of environmental conditions, screening and isolation of cells, and cultivation of a variety of microbial species. Finally, we highlight how the MM enabled discoveries in a wide range of fields in microbiology, such as cell-size control, genetic mutations, cellular aging, stress responses, cell-fate determination, antibiotic tolerance/ persistence, and synthetic biology. For more details, we refer the interested reader to previous reviews that have comprehensively described device fabrication and setup[102–104], discussed challenges associated with single-cell analysis[92,105], and reviewed different microfluidic devices[102,106–110].

2.4 Technical developments of the mother machine

2.4.1 Original design and challenges

Performing experiments with the MM requires the following: designing and fabricating a mold for the device, building a microfluidic chip, performing the time-lapse microscopy, and analyzing the images to create time traces. Here, we start with an overview of the original MM design and the challenges that motivated recent technical developments.

2.4.2 Device design and fabrication

The original MM design was developed to study *Escherichia coli* cells[82]. Narrow trenches trap bacterial cells perpendicular to a larger feeding channel that allows media to deliver nutrients to the cells and wash away progeny emerging from the trenches (Figs 2.1A,B). Several constraints must be considered in the design: the width, height, and length of cell trenches, spacing between cell trenches, and dimensions of the feeding channel. The width and height of the trenches are approximately the dimensions of the particular strain of bacteria being cultivated (e.g., 1.2 μm height, 1.3 μm width, and 20 μm length for E. coli MG1655). Proper trench dimensions ensure that the cells are in focus, restrict growth to single file within each trench, and ensure sufficient diffusion of nutrients to all cells in a trench. Too large of dimensions results in cells overlapping each other in the z direction–making segmentation and tracking hard to impossible. Too small of dimensions leads to difficulties loading the cells into the trenches and results in poor nutrient diffusion to cells deep in the trenches, including the mother cells. The chosen length of a cell trench is a trade-off between cell retention over time, as short trenches lose cells more rapidly (e.g., through stochastic filamentation that pulls them out in the feeding channel), and feeding of the mother cell. It is thus important to ensure that the growth rate of the mother cell is the same inside the device and in batch culture for each strain and device combination[111]. Spacing between cell trenches is a trade-off between the throughput (i.e., number of lineages followed per image) and accuracy of fluorescence measurements. Trenches too close to one another can result in biased fluorescence measurements, particularly if neighboring trenches have very different signal intensities[92,112]. Finally, the width and height of the feeding channel are chosen to minimize hydraulic resistance to facilitate the flow of growth medium, e.g., with syringe pumps. A single centimetre-sized chip can typically fit

multiple channels, each with their own inlet and outlet, to enable simultaneous experiments with multiple strains (Fig 2.1A).

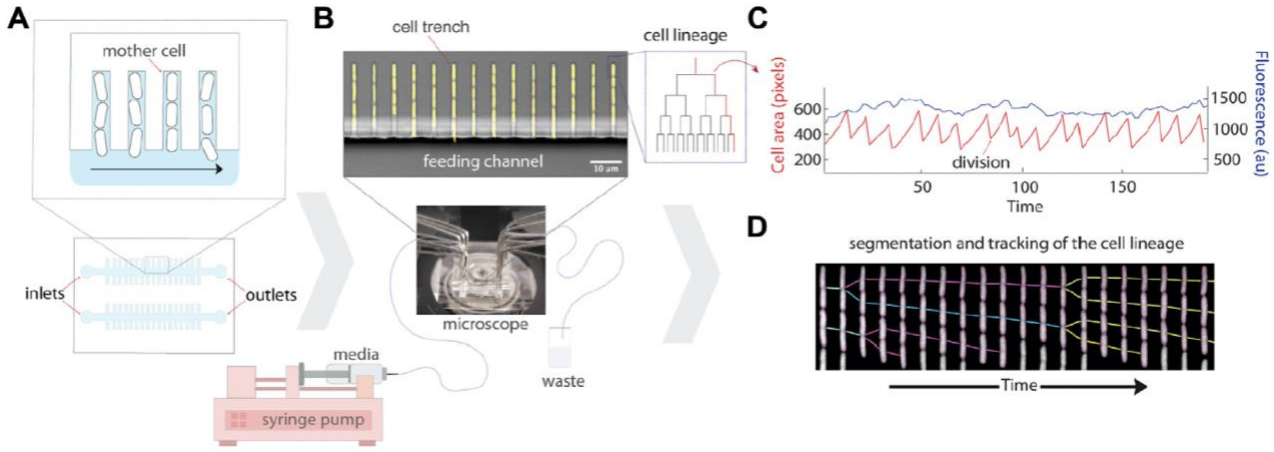

Figure 2.1 Schematic of the experimental setup for the mother machine microfluidic device and data analysis. **(A)** Schematic representation of the platform which traps single bacterial cells in trenches that are perpendicular to a larger feeding channel. Daughter cells are flushed out of the trenches with flowing media, while mothers remain trapped at the end of the cell trench. **(B)** A micrograph of the mother machine, with YFP fluorescence showing the cells superimposed on a brightfield image of the device. Media is pumped through the inlet into the main feeding channel by a syringe pump, and then exits through the outlet into a waste beaker. **(C)** The lineages of growing cells in the trenches can then be followed under precisely controlled environmental conditions using time-lapse microscopy. **(D)** An example kymograph of a growing cell imaged in fluorescence, illustrating the segmentation and tracking of the lineage.

After the design is finalized, a mask can be drawn using CAD software and ordered through different companies (e.g., Toppan Photomasks, United States). The mold is then built on a silicon wafer in a cleanroom environment using photolithography techniques, where the mask is used to expose photo-sensitive resin to light to define the features[102,104]. The mold is a negative of the features of the chips (i.e., what is solid on the mold becomes air in the device). The ~1 μm-sized features are on the lower end of the resolution of these techniques, and smaller features (e.g., Section 2.4.7) require other fabrication techniques (e.g., electron beam lithography). As such, fabrication protocols typically require fine-tuning to obtain the critical feature size (cell trench width and height) within a ~0.1 μm range, which can affect the experiments as described above. However, once built these molds can be re-used indefinitely to build microfluidic chips. Alternatively, the mold can be ordered custom-built from companies such as: ConScience

(Sweden), Cornell NanoScale Science and Technology Facility (United States), Innopsys (France), Kavli Nanolab Delft (Netherlands), Micro Resist Technology (Germany), Sigatec (Switzerland), and TTP (UK). Molds can also be duplicated in epoxy, which can be an inexpensive option for sharing molds between groups[113].

2.4.3 Experiment setup

The MM microfluidic chip is made by pouring and curing polydimethylsiloxane (PDMS) on top of the mold, imprinting the features of the mold onto the chip. Individual chips are then cut out of the PDMS slab, and holes are punched (e.g., with biopsy punchers) at the inlets and outlets to allow the connection of tubing which provides growth medium to the device. The chips are then covalently bonded to a coverglass using plasma treatment. Cells can then be loaded into trenches via centrifugation with a custom adapter, or by simple diffusion by loading a very dense culture. Tubing is connected to the inlets and outlets (e.g., using syringe needles) for flow of fresh growth media into the chip, as well as removal of used media which has passed through the chip (Fig 2.1B). The media is typically pushed through the device using syringe pumps, initially at a high flow to clear biofilm that may be growing in dead spaces (i.e., regions of low flow) in the inlets and outlets. The formation of biofilms can be limited by pre-coating the chip with bovine serum albumin (BSA) and/or supplementing the growth media with BSA or Pluronic[95,114]. The chip is then mounted on an inverted fluorescence microscope for automated time-lapse microscopy of the lineages growing in the trenches. A cage incubator and hardware autofocus are typically required to ensure stability of the focus over multiple days. Detailed protocols for setting up MM experiments have been published[114]. After the experiment, the multi-dimensional images (position, fluorescence channels, time) can be processed to track the properties of single lineages growing in the device (Fig 2.1C; Section 2.4.5).

2.4.4 Challenges

The original design of the device enabled time-lapse microscopy of single *E. coli* cells under controlled growth conditions, leading to many biological discoveries. There are however some challenges associated with the experimental setup, which have led to new technical developments discussed below. For example, automated image processing traditionally required

constitutive expression of a fluorescent protein (FP) at intermediate levels specifically for that purpose. This limited the number of simultaneous reporters that could be used in an experiment, while also preventing the study of bacteria not expressing exogenous FPs. Section 2.2 describes the recent tools developed for segmentation and tracking of cells using phase contrast images. In addition, the original setup of the MM makes switching conditions within an experiment challenging. With this design, growth media can be changed using a Y-junction close to the chip, although this creates a short (and imprecise) delay in the switch as the medium between the Y-junction and the chip is being replaced. Creating complex environmental conditions within the chip, i.e., by flowing a growing culture, can be challenging due to the introduction of air bubbles into the feeding channel. Such challenges have inspired the development of more sophisticated fluidic and environmental control strategies, which are detailed in Section 2.4.6. Another limitation of the original design is the inability to genotype or isolate cells within the device, which can be useful when imaging libraries of cells. While phenotyping pooled genetic libraries is possible in the device, isolating single cells of interest from the conventional MM platform has been impractical due to the inevitable formation of biofilms in the inlets and outlets, which additionally limit the total duration of an experiment. While cells could potentially be genotyped on-chip through fluorescence in situ hybridization (FISH) techniques, diffusion of probes through the cell trenches makes this process inefficient. These limitations have led to the development of techniques for single-cell screening detailed in Section 2.4.7. Finally, the original device was limited to culturing *E. coli* or other similarly sized microbes. Modifications to trench dimensions and the addition of other features have now allowed the growth and imaging of a variety of other microbes. The cultivation of some species requires additional modifications, which are further described in Section 2.4.8.

2.4.5 Segmentation and tracking algorithms

While the experimental techniques for using the MM have become increasingly accessible, the image analysis pipeline to convert time-lapse images into single-cell traces through segmentation and tracking has lagged. For many years, laboratories using the MM have developed their own customized data analysis pipelines. While tools have been developed for tracking the growth of microbes on agar pads using phase contrast[115], the large features of the MM PDMS chip can confound such image analysis tools. Recently, multiple open-source software packages have

been published specifically for MM experiments with the capability of performing the segmentation and tracking on phase contrast images (listed in Table 2.1).

Most of these image analysis methods share a common overall workflow: pre-processing of the images, segmentation of the cells, and tracking the lineages. In the pre-processing step, the image time series are first registered to correct for drift and jitters of the stage, for example, using cross-correlation between successive images. The images are rotated to align the microchannels vertically, which simplifies further analyses. The microchannels are then identified and segmented. Accurately segmenting individual cells is typically the most challenging task, as the cells are small and in contact with each other, and strategies vary between implementations. Tracking is then performed to create time traces of individual cells, where cells from each time point are connected to the cells in the next one, and cell divisions are identified (Fig 2.1C). Properties such as cell size and fluorescence intensity are extracted along these single-cell time traces. Finally, a manual curation pipeline is typically available, as even rare segmentation and tracking errors can have large effects on sensitive measurements such as the variance.

Table 2.1 Overview of open-source software packages developed for mother machine segmentation and lineage tracking. The applicability to specific imaging modalities indicates which ones have been demonstrated. All programs are available on Github or Gitlab.

Software	Language	Deep learning based	Phase contrast segmentation	Brightfield segmentation	Fluorescence segmentation
Molyso (Sachs *et al*., 2016)	Python		✓		
MoMA (Kaiser *et al*., 2018)	Java		✓		✓
MMHelper (Smith *et al*., 2019)	Python		✓	✓	
BACMANN (Ollion *et al*., 2019)	Java		✓		✓
DeLTA (Lugagne *et al*., 2020; O'Connor *et al*., 2022)	Python	✓	✓		
DistNET (Ollion and Ollion, 2020)	Python	✓	✓		

In Molyso[116], the cell segmentation is done in one dimension with cells identified by bounding rectangles instead of cell contour. The tracking is done by solving an optimization problem, where a cost is imputed for cell displacement between time points and cell division events. MoMA generalized the optimization problem for both the segmentation and tracking, overpredicting possible cell segmentation and performing the tracking simultaneously[112]. This 1D segmentation works well when the cells are perfectly aligned with the channels. However, it can result in errors when the cell width is smaller than the channel width, resulting in tilted cells, or if the cells are not perfectly rodshaped (e.g., mutants or other bacteria with different morphologies). BACMANN enables 2D segmentation (i.e., cell contour) through watershed-based image processing techniques, while the tracking is based on the position with respect to the top of the trench[117]. BACMANN also incorporates a spot-tracking algorithm in its pipeline. MMHelper was developed using similar segmentation approaches to also segment using bright-field instead of phase contrast[118]. DeLTA[119] utilizes 3 U-net convolution neural networks[120] to perform channel identification, cell segmentation, and tracking. DistNET incorporates a self-attention layer into the

U-net architecture to provide information about the whole channel to the neural network, and performs segmentation and tracking through one deep neural network[121]. Comparison of BACMANN, DeLTA, and DistNET on the same dataset showed that they could achieve <1% combined segmentation and tracking error rates[121]. While BACMANN's tracking performed better than DeLTA, DeLTA's segmentation performed better. DistNET's self-attention layer mainly improved the tracking performance of DeLTA. Benchmarking the techniques against data from different experimental conditions showed good performance but an increased error rate, suggesting a need for more training data or for changing the analysis parameters[121].

When choosing a program, we encourage users to consider the following criteria: accuracy of segmentation and tracking, need for manual curation, speed of analysis, quality of documentation, readability of code, ease of use, flexibility to specific experimental needs, and an actively maintained codebase. Deep-learning methods can be fast and very accurate while requiring training on a relatively small set of manually analyzed data. However, they often lose accuracy when the experimental conditions are different from the training set (i.e., cell size, trench width, etc.). Conventional methods typically require changing analysis parameters to accommodate these kinds of changes, but that can be less tedious than manual segmentation of many images required to re-train a deep-learning algorithm. Generating synthetic data to train the neural networks would greatly alleviate their main shortcomings.

2.4.6 Fluidic control and environmental conditions

One key strength of the MM is the precise control over the growth conditions. However, switching between conditions within an experiment and flowing mixed media are challenging using the original design. A rapid and precise switch between growth media can be obtained by modifying the device design to include two inlets for each feeding channel. To flow a mixture of media, it is necessary to introduce a serpentine channel between the inlet and the feeding channel to overcome the mixing limitation of the low Reynolds number environment. The dual input mother machine (DIMM, Fig 2.2A) utilized this strategy to study the induction of the lac operon while switching from glucose to lactose[112]. The authors could track the lag in growth of single cells exposed to this transition and found that the distribution of the growth lag was multi-modal. By quantifying the number of LacY/Z ("sensor") molecules in single cells in the device, this

multimodality was subsequently attributed to a fraction of the population expressing zero LacY/Z molecules, relying instead on stochastic leaky expression for induction of the operon[122]. However, any number of expressed lacY/Z molecules was sufficient for fast induction of the operon, making it a single-molecule trigger.

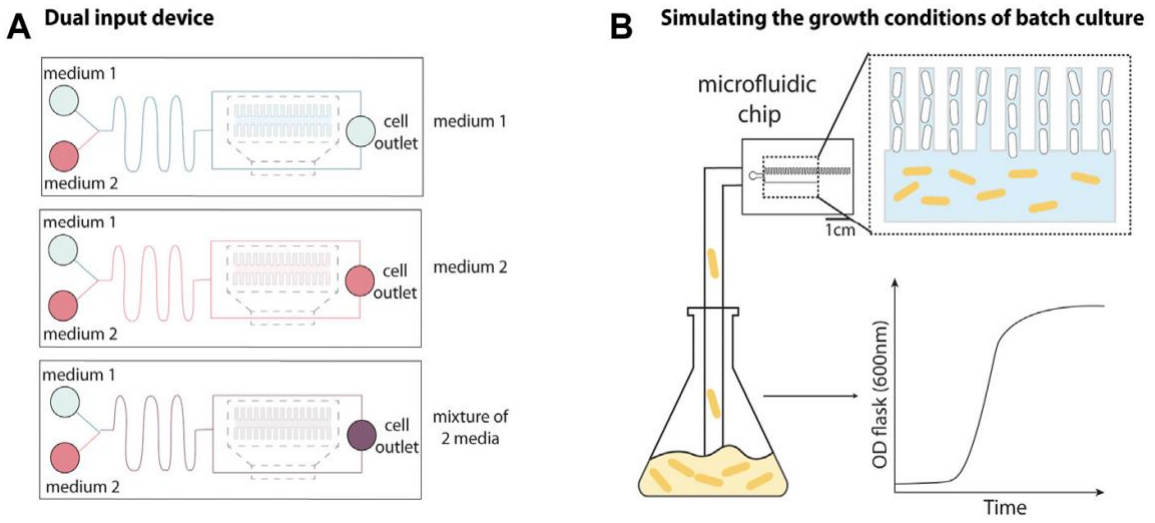

Figure 2.2 Adaptations to the mother machine architecture for improved fluidic and environmental control. **(A)** The dual input mother machine (DIMM) has two media inlets followed by a serpentine channel that fluid passes through prior to reaching cell trenches to facilitate mixing and/or rapid switching between different environmental conditions. Schematic representation inspired from Kaiser *et al*. (2019). **(B)** The growth curve platform allows batch culture to be fed into the device to recapitulate batch culture conditions. This allows for observation of cells entering and exiting the stationary phase by switching between nutrient depleted culture and fresh media. Schematic representation inspired from Bakshi *et al*. (2021).

An experimental setup was developed to mimic the conditions of batch culture (Fig 2.2B), where a growing culture is flowed directly into the microfluidic device, enabling the study of cells transitioning between different growth phases[123]. This was achieved using peristaltic pumps to flow a culture growing in a separate shaker-incubator into the device, and bubble traps to prevent air bubbles from entering the device. By alternating between flowing fresh media and batch culture into the MM, the authors monitored cells after multiple rounds entering and exiting the stationary phase and found that the cell-size regulation strategy changed throughout phases of the growth curve (discussed in Section 2.5.1).

2.4.7 Screening and isolation based on time-lapse microscopy

Genetic screens have been instrumental in biology for assigning function to molecular components and generally linking genotypes to phenotypes. Many powerful screening platforms have been developed, but they have been mostly limited to distinguishing static phenotypes in the population. Recent technical developments have transformed the MM into a powerful platform that combines dynamic phenotype screening with genotyping or isolation capabilities. This enables screening based on dynamic and/or spatially resolved phenotypes, such as oscillations in gene expression, cell-size control mechanisms, response to changes in environmental conditions, and intracellular localization of proteins. Notably, even static phenotypes could be isolated more precisely because cells can be quantified over many generations, and thus genetic and nongenetic heterogeneity could be distinguished.

Two techniques have been developed to date for screening cells in the MM. The first technique, named "dynamic μ-fluidic microscopy-based phenotyping of a library before in situ genotyping" (DuMPLING)[124], enables dynamic phenotyping of pooled libraries. After characterization of the library in the MM, the cells of the barcoded library are fixed and identified via fluorescence in situ hybridization (FISH), connecting genotypes to dynamic phenotypes (Fig 2.3A). A 300 nm gap at the dead-end of the trench is connected to a back-end channel, which generates convective flow that facilitates efficient movement of probes and media over the cells. This convective flow also facilitates feeding of the mother cell therefore reducing the diffusion limitations related to the dimensions of the cell trenches discussed in Section 2.1.1. The DuMPLING platform was used to identify the effects of a CRISPR interference-mediated gene knockdown library on the coordination of replication and division by tracking chromosome replication forks throughout cell division[125].

The second technique, named single-cell isolation following time-lapse microscopy (SIFT)[126], uses a modified microfluidic chip containing an additional media channel used for cell isolation (Fig 2.3B). The device has a system of pressurized valves that separates the cell trenches from the collection channels, temporarily closes the inlets and outlets for sterilization, and closes the media channel to stop the liquid flow. This enables an optical tweezer to move cells of interest

from their growth trench to a collection trap where they are isolated, cultured, and sequenced. SIFT was used to screen two libraries of synthetic genetic oscillators based on the periodicity and precision of oscillations, showcasing its strength in isolating dynamic phenotypes.

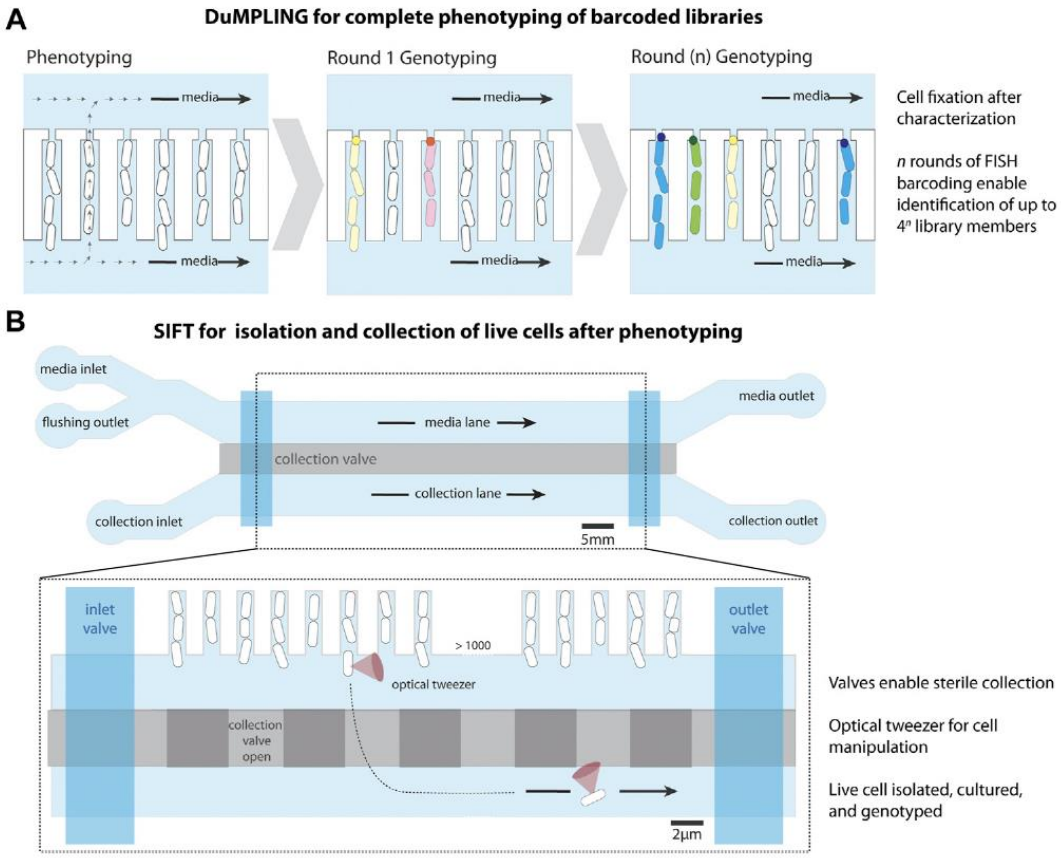

Figure 2.3 Modifications to the mother machine to enable cell screening. **(A)** Dynamic u-fluidic microscopy-based phenotyping of a library before *in situ* genotyping (DuMPLING) has a 300 nm gap at the end of the cell trench, allowing media to flow through the cell channels. Rounds of barcoding through FISH enable genotyping of the pooled library. Schematic representation inspired from Lawson *et al*. (2017). **(B)** Single-cell isolation following time-lapse microscopy (SIFT) uses a modified microfluidic chip containing an additional lane for cell isolation below the cell trenches, separated by a pressurized valve system (collection valve). A second set of valves (inlet and outlet) allows for the lane to be sealed for inlet cleaning and restricting media flow after cell loading. An optical tweezer moves cells of interest from their trench to a collection trap, where they are isolated and removed from the device to be cultured and sequenced. Schematic representation inspired from Luro *et al*. (2020).

Both of these screening techniques have advantages and disadvantages. While DuMPLING enables the *in situ* genotyping of entire libraries and allows genotype-phenotype mapping across a large number of cells, it requires a barcoded library and cell fixation prior to hybridization, thereby eliminating any possible downstream growth and analysis[124]. Conversely, SIFT does not require barcode labeling, enabling the screening of unmodified libraries and natural populations, the isolation of live cells, and downstream analysis of isolates[126]. However, only isolated cells can be genotyped, limiting the scale of phenotype-to-genotype mapping throughput. Additionally, the optical trapping mechanism in this technique requires an extensive platform. These extended capabilities for screening and isolating cells within MM-like devices have the potential to enable discoveries in diverse fields of microbiology.

2.4.8 Extension to other microbes

Adaptations to the MM have enabled single-cell studies of a variety of microbes. In principle, adaptation of the MM design to other symmetrically dividing organisms should only be a matter of adapting the trench size, although other minor modifications may be necessary to maintain species-specific optimal growth conditions. Such devices have been fabricated for cultivation of *Corynebacterium glutamicum*[116] and *Bacillus subtilis*[114,127]. *As B. subtilis* stochastically forms long multicellular chains which would be pulled out of the trenches, an adaptation of the classic MM device incorporated an increased trench length of 75 μm[127]. This two-layer device included shallower feeding channels surrounding the cell trenches to ensure sufficient feeding of cells at the end of these long trenches (Fig 2.4A).

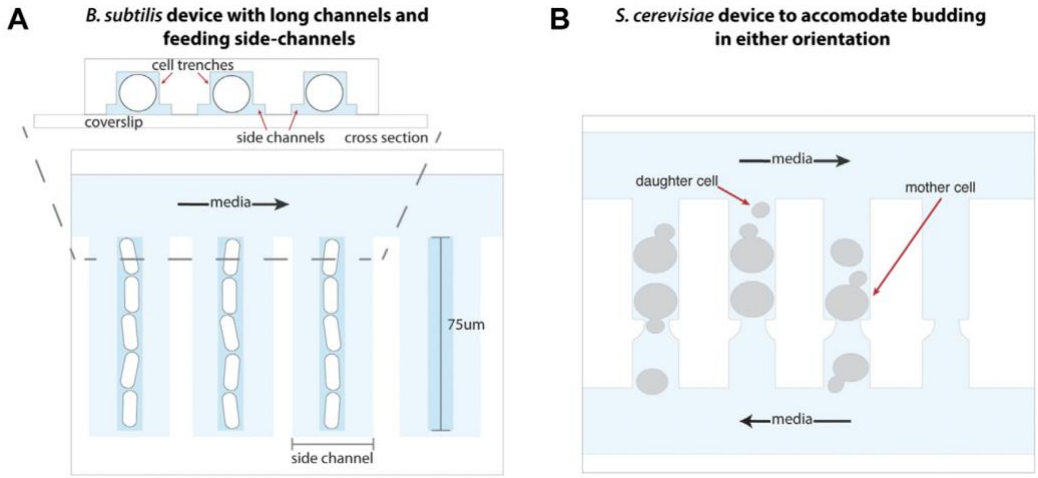

Figure 2.4 Adaptations to the mother machine architecture to optimize growth of other organisms. **(A)** The mother machine design adapted for *B. subtilis* growth includes elongated trenches 75 μm in length to accommodate its multicellular, chained state, as well as side channels that enable uniform nutrient availability throughout the trenches. Schematic representation inspired from Norman *et al*. (2013). **(B)** Maintaining an opening at either end of each cell trench in a modified mother machine device enables removal of *S. cerevisiae* daughter cells produced from budding in either orientation into perpendicular media channels. Schematic representation inspired from Li *et al*. (2017).

The classic MM architecture has been used to study archaea and symmetrically-dividing yeast organisms such as *Halobacterium salinarum*[128] and *Schizosaccharomyces pombe*[129], respectively, by scaling up device dimensions. The ability of the budding yeast *Saccharomyces cerevisiae* to switch budding orientation over the course of its lifespan necessitated the trapping and retention of mother cells in trenches open on both ends to flowing media[130]. This accommodates the removal of daughter cells produced by budding in either orientation (Fig 2.4B). Alternatively, the "yeast jail" design forgoes trenches altogether and instead employs a microfluidic device with an array of jail units[131]. Each jail is composed of three PDMS posts (among other designs) that behave as "jail bars" to retain a single mother cell, while daughter cells produced by budding are washed away with the flow of media. Similarly, A Long-term Culturing And TRApping System (ALCATRAS)[132], High-throughput Yeast Aging Analysis chip (HYAA)[133], and slipstreaming MM[134] devices comprise an array of PDMS trapping units, many of which may fit into a single field of view during imaging, to enable tracking of individual mother cells over their lifespan. In the latter, *S. cerevisiae* cells are loaded through the outlet of the device such that media flow reversal enables the trapping of mother cells in a low-pressure zone behind

PDMS pillars. This method is ideal for studying cell replicative life span as it does not place cells under mechanical pressure during trapping, and the effect of such stress on aging is not yet known. An alternative method utilizes channels or PDMS structures of optimal heights for trapping mother cells underneath them, while permitting smaller daughter cells to be flushed away[135–137].

2.5 Applications to study bacteria

Several features of the MM have facilitated important discoveries about a variety of cellular processes. The tracking of single cells under controlled and tunable growth conditions with high throughput has shed light on how cellular processes are affected by stochastic gene expression, and how such heterogeneity can affect the cell's phenotype. The ability to track the same cells for many generations has facilitated studies in cellular aging, and an inherent lack of competition between cells in the device has proven useful in studying genetic mutations. Here we will highlight discoveries about cell-size control mechanisms, genetic mutations, cellular aging, stochastic pulsing of gene expression, phenotypic states in *B. subtilis*, antibiotic resistance and persistence, and synthetic biology that have been enabled by the MM platform. Instead of a detailed description of each study, we highlight how the device has enabled such discoveries.

2.5.1 Cell-size control

Most prokaryotes divide via binary fission, yielding two daughter cells of nearly identical size and volume[138]. If left unchecked, small fluctuations in cell size at cell division can result in significant size divergence between cells of a population over successive generations. Cell-size homeostasis could in principle be achieved through different control mechanisms[139]. Several studies have shown that *E. coli*, *B. subtilis* and *Caulobacter crescentus* maintain cell-size homeostasis by behaving primarily as "adders", adding on average a constant length between birth and division, rather than as "sizers" or "timers", for which cell division is triggered upon cells growing to a threshold size or for a fixed time, respectively[140–143]. As time-lapse microscopy on agar pads is limited to a few cell divisions where the growth conditions can change, microfluidic approaches have been important in studying cell-size regulation. The ability to image hundreds of single cells under constant growth conditions while precisely measuring their size throughout the

cell cycle (e.g., size at birth and added during the cell cycle) has made the MM a particularly useful platform in elucidating the specific mechanisms underlying cell-size regulation[144–148].

Several models have been suggested to explain the mechanism underlying adder behavior[146–150]. While a detailed description of the different models is outside the scope of this review, a recent analysis by Le Treut et al. has found the authors' model, the independent double adder, to be the most consistent with current data[151]. This model proposes that the processes of cell division and initiation of DNA replication are controlled by distinct (independent) adders[146]. It further suggests that the mechanism underlying this type of cell-size control relies on accumulation of specific initiator proteins for independent regulation of cell division and DNA replication to a certain threshold and that they are produced at a rate proportional to cell growth without being actively degraded. This hypothesis was supported by experiments that used the MM to measure the cell size added between cell divisions, and the cell size added between DNA replication initiation events (tracked with DnaN-YPet)[146], which were both found to be independent of initial cell size (i.e., adders). Perturbing the production of each initiator protein (FtsZ and DnaA respectively) only dysregulated cell-size control for its respective process.

Some studies carried out in the MM have shown deviations from the adder principle under slow growth conditions[143,146,148]. Si et al. (2019) suggest that the adder principle can be broken if the underlying mechanisms (threshold and constant production) are affected. They suggest that active degradation of the division initiatior (FtsZ) could play that role, and elimination of degradation through clpX repression restored the adder phenotype under that growth condition[146]. A recent study used a variation of the MM setup which flows batch culture into the device as a means of replicating conditions within that culture on-chip to monitor *E. coli* and *B. subtilis* growth, and revealed that cells alter their size regulation strategy as they progress through different growth phases[123]. Cells switched to mixed "adder-timers" while they entered the stationary phase and behaved as "sizers" while exiting the stationary phase, suggesting that different strategies might be used to respond to changes in environmental conditions. These results also highlight the importance of using the MM for studying this process, as other single cell imaging techniques such as agar pads do not offer precise control over environmental conditions. Developments in the control of growth conditions as well as screening capabilities will thus facilitate the development of more

complete models that can capture cell-size control strategies under varying environmental conditions.

2.5.2 Genetic mutations

Mutations and other DNA damage events such as double-stranded breaks (DSBs) have the potential to drastically affect cell survival and fitness if left unrepaired[152]. To counter such mutations, *E. coli* employs effective DNA repair pathways to recognize and repair genetic perturbations before they are propagated to future generations. The ability to track thousands of lineages in parallel (without growth competition between individuals) makes the MM an ideal platform to study rare events such as the emergence of DNA mutations. Its capacity to capture heterogeneity in number and types of mutations emerging between isogenic cells of a population further highlights the utility of such single-cell, time-lapse studies. To this end, the MM has been used to visualize copy number variations[153], DNA mismatch error[154,155], DSBs[156], and alkylation damage[157–159].

The timing of mutations as well as their impact on the fitness of the cells are important variables in the process of evolution. The rate of chromosomal gene copy number mutations in *E. coli* was estimated at ~3 x 10^{-3} per cell per generation in the MM[153]. This was achieved by expressing several copies of a chromosomally integrated fluorescent reporter and measuring changes in fluorescence over time as an indicator for gene copy number (because gene expression is roughly proportional to gene copy number). Robert et al. leveraged the lack of competition in the MM to visualize the appearance of DNA replication errors and their fitness impact[154,155]. To measure the fitness effect of the mutations, they measured the decrease in growth rate (i.e., fitness) of the individual lineages through the accumulation of mutations[154]. Instantaneous single-cell growth rate can be calculated in the MM using the relative change in cell size between successive time points (i.e., doubling rate). Although the entire distribution of fitness effects (DFE, which has proven challenging to measure in the field of evolution modeling) was still not directly estimated, the authors were successfully able to infer all the moments of DFE (i.e. average, variance, skewness, etc.) - thanks to the ample statistics enabled by the MM. The analysis indicated the underlying distribution to be long-tailed, with most mutations having little-to-no cost on cell fitness: mean fitness cost was only ~0.3 %, which was apparently overestimated by the previous

studies. In contrast, 1% of the mutations were found to be lethal, directly measured by observing cell death in the MM. Mutations were detected by tracking the appearance of YFP-MutL foci, and occurred at a constant rate over time during steady state exponential growth, as expected from a memoryless Poisson process. However, another MM study showed that a subset of cells within a population exhibited a period of elevated mutation rates in response to DNA alkylation damage, due to delayed activation of the Ada DNA damage response regulon[158,159]. These periods of high mutation rate lasted several generations, since many cells had no sensor-activator Ada molecules present, and had to wait for stochastic expression to induce the response[157]. Finally, the response to DSB has also been characterized using an adapted MM with multiple inlet ports connected to the feeding channel via a short junction, enabling rapid switching between different media[156]. Switching between a growth medium and an induction medium enabled short induction of Cas9, which created a targeted DSB in the chromosome. The chromosomes could be tracked using fluorescently-tagged proteins (ParB and MalI) with DNA-binding sites localized close to the DSB, with the foci disappearing during the DSB. Repairs were rapid (~15 min), homogeneous, robust (~95% of cells repaired the damage), and had low impact on the fitness of the cells. This is impressive given that the DSB needs to find/colocalize with its repair template on the sister chromosome. The RecA-single stranded DNA complex was observed to extend in a long filament spanning the length of the cell. This could facilitate the homology search for the repair template by eliminating the need to search along the length of the cell in the z direction, thereby reducing it from a 3D problem to a 2D one and making the search process 100 times faster.

2.5.3 Aging

The phenomenon of aging in unicellular organisms is broadly described in terms of senescence, or the progressive loss of fitness over time[160]. This loss of fitness can be due to a decrease in growth rate and/or an increase in death rate. Defining the 'age' of a unicellular organism that lacks replicative asymmetry can be challenging, but generally takes into account the asymmetric segregation of damage factors during cell division, which creates effectively 'older' and 'younger' progeny cells. For example, in budding yeast asymmetric division creates a finite replicative lifespan by partitioning detrimental cellular factors such as misfolded protein aggregates to older 'mother' cells, while preserving the daughter lineage[161]. The mother exhibits senescence over successive generations and eventual cell death. While *E. coli* divides symmetrically, there is

still an intrinsic asymmetry in the process: one pole is created during division (the 'new' pole), and one is left intact (the 'old' pole)[162]. Asymmetries in partitioning of cellular contents have also been observed in *E. coli*. For example, the main efflux pump (AcrAB-TolC) was shown to be partitioned with a bias for the old pole cell, leading to elevated efflux activity in 'older' cells[163]. Non-random segregation of sister chromatids has also been observed, with the ancestral strand being partitioned preferentially in the old pole cell[164]. The MM is uniquely suited to study aging in symmetrically dividing bacteria as it retains an old pole cell at the end of each trench over an entire experiment, thus facilitating monitoring of the old pole lineage for many generations. Here, we present findings from several studies monitoring the aging process in *E. coli* in the MM, where the age of a cell is defined as the age of the old pole.

Both decreased growth rate and increased death rates have been associated with aging in *E. coli*[82,165–167]. The first report of the MM studied the aging of the mother cell over consecutive generations[82]. They found that the growth rate of the mother cell was stable for more than a hundred generations, but observed that the filamentation rate increased until 50 generations[82]. Note that in 50 generations of exponential growth, 1 cell would divide into ~1015 cells, making such studies intractable without the use of devices like the MM. Subsequent studies tracked the growth rate of both the mother cell and its immediate progeny, the 'daughter' cell. This showed that these cells reached different equilibrium growth rates, with the mother cell stabilizing at a growth rate slightly slower than the daughter cell[162,166]. This suggests that damaged molecules divided asymmetrically, with a preference to the old pole cell. The nature of this damage and the mechanisms underlying asymmetrical partitioning of cellular components are under investigation. Misfolded proteins are a prime suspect, as a chaperone fusion (IbpA-YFP) was shown to preferentially localize to the old pole as a foci[165,166], while protein stress such as phototoxic stress affected the asymmetry[166]. However, FP fusions such as YFP have been shown to create artifactual foci due to their oligomeric properties[168]. Therefore, the use of FP fusions that do not cause aberrant foci (e.g., ClpB-msfGFP) will be informative in tracking protein aggregates[169]. In contrast, another study has shown no asymmetries in misfolded protein aggregates using brightfield imaging for inclusion bodies and ThT dyes to visualize protein aggregates[167]. Asymmetric retention of protein aggregates at the old pole has also been observed in the symmetrically dividing fission yeast *S. pombe* in a MM-like device[129]. These aggregates were not associated with increased division times and were eventually

transferred to a new daughter, thereby rejuvenating the old lineage. While it is clear that even cells dividing "almost symmetrically" like *E. coli* exhibit aging, the elucidation of the molecular mechanisms and the agents causing this phenomenon will shed light on the universal properties of cellular senescence, and the MM provides an ideal platform with which to study it.

2.5.4 Stochastic pulsing

Stochastic fluctuations in gene expression can drive phenotypic heterogeneity among clonal bacterial populations, such that genetically identical cells display distinct behaviors. The use of FP reporters for gene expression have been invaluable in quantifying this heterogeneity. In principle, this heterogeneity can be generated on different timescales. For example, cells can stochastically express genes at different levels for long periods of time (e.g., stable epigenetic state), or they can fluctuate rapidly between these different expression levels (e.g., rapid pulses). Long-term timelapse microscopy using microfluidic devices such as the MM enables tracking the expression dynamics in thousands of individual cells under controlled growth conditions and can elucidate the timescales of such fluctuations. Employing this strategy, it was shown that the promoters controlling flagellar biosynthesis genes in *E. coli* activate in stochastic pulses even if expression of their master regulator was constant[170]. Measuring expression of a gene (*bolA*) dependent on the *E. coli* general stress response factor, RpoS, revealed heterogeneous expression in liquid culture, in the MM, and in another microfluidic device[171]. The promoter activity (production rate of the reporter) can be calculated using the derivative of the fluorescence intensity while accounting for dilution of the FP present[172]. The promoter activity revealed stochastic pulses of expression which coincided with periods of slower growth in the device[171]. The ability to rapidly change environmental conditions andmeasure single-cell properties prior to and after the change enabled them to test whether these periods of slow growth led to increased resistance to stress. They observed that cells with higher RpoS activity and slower growth immediately prior to the stress were more likely to survive a hydrogen peroxide treatment. Another study measured the expression of multiple stress response genes in the MM and found additional RpoS-dependent promoters exhibiting stochastic pulses that negatively correlated with growth rate[64]. Genes from the SOS regulon also displayed pulsatile activity, but these were not correlated with the growth rate. Cells undergoing pulses of genes from both these groups prior to a short treatment of the antibiotic ciprofloxacin in the MM had increased

likelihood of survival[64]. Pulses in the SOS regulon have also been observed in another study using the MM, and have been attributed to variability in the degradation of its regulator, LexA[173].

In *B. subtilis*, several sigma factors have been reported to exhibit stochastic, pulsatile bursts of expression[55,172,174], which can be similarly tracked in the MM. Sigma factors in *B. subtilis* promote the production of their own operons, which also encodes their anti-sigma factors, creating positive and negative feedback that can cause pulses of gene expression. Molecular "time-sharing" was proposed as a mechanism in which alternative sigma factors competing for RNA polymerase binding opportunities are able to share such core resources over time[55]. Stochastic bursts of sigma factor activity also seem to play a role in stress response in *B. subtilis*: heterogeneous response to lysozyme stress was observed between individual cells grown in the MM[175]. Pulsatile expression of the sigV operon preceding exposure to lysozyme stress led to increased survival probability.

2.5.5 Phenotypic states in B. subtilis

Early work with *B. subtilis* in the MM revealed the existence of a cell fate switch controlling whether *B. subtilis* exists in a free-living, motile state or as a sessile member of a multicellular chain associated with biofilm formation[127]. A modified device was used, with side-channels to ensure even nutrient availability in the long channels that accommodate the chain phenotype. By tracking the fates using fluorescent reporters over hundreds of cell generations, it was found that the transition from the motile to the sessile state happened at a constant rate over time (i.e., is a memoryless process), but the cells spent a precise amount of time in the sessile state. A simple network of three proteins could recapitulate all the properties and the modularity of the switch and the commitment to the chained state. Remarkably, the circuit was reconstituted in evolutionarily distant *E. coli*, showing that this simple network is sufficient to drive cell-fate decision making[176]. The stochastic entry into another cell fate–sporulation–was also studied using the MM, and was shown to occur at a constant rate over time after adaptation to the sporulation-inducing conditions[177].

In another study, a clonal *B. subtilis* population diverged into subpopulations of distinct metabolic specialists, each characterized by differential expression of metabolic genes[56]. Cells with stochastically upregulated *sucC* expression in mid to late exponential phase were associated with

the production of acetate, while a subpopulation expressing *alsS* in early stationary phase was linked to production of acetoin. Cells could be observed stochastically switching in and out of such states with fluorescent reporters in the MM. As acetoin can neutralize low pH conditions caused by acetate accumulation, the slow-growing *alsS*-expressing subpopulation enabled growth and expansion of an *alsS*- subpopulation which benefited from the neutralization of acetate in an agar pad microenvironment. This showcases how stochastic gene expression can help populations of genetically identical cells achieve cooperative behaviors. Therefore, bacteria have shown the ability to harness molecular fluctuations through simple circuits of a handful of proteins to establish heterogeneous phenotypic states that can be advantageous to the bulk isogenic population.

2.5.6 Antibiotic resistance and persistence

The rise of antibiotic resistance combined with the lack of new antibiotics is an alarming threat to public health[178]. Persister cells can survive antibiotic treatment by remaining in a temporary state of dormancy throughout antibiotic exposure, without being genetically resistant[179]. The switch to this state can happen spontaneously or be induced by stress such as starvation. Microfluidic devices are particularly well-suited for the study of this non-genetic heterogeneity since growth conditions can be precisely controlled and single lineages tracked over time. One of the first applications of a MM-like device was to establish the persister state as a phenotypic switch[93]. Persisters can be identified in such microfluidic devices as cells that are not growing prior to antibiotic exposure, but resume growth at some later time point following removal of the antibiotic. With an increase in throughput of the MM and microscopy (e.g., more trenches per chip and faster microscope imaging with larger field of view), it was possible to observe hundreds of *E. coli* persisters without mutations that increase their typically low frequency of approximately 1 in 1000 cells[123]. The molecular mechanisms underlying this phenotypic switch are still under investigation[180,181]. Studies using the MM enabled the characterization of these persisters and have shown that they have smaller size[123], lower ATP levels[181], and are more likely to contain protein aggregates[182]. Recent developments in microscopy throughput, simulating batch culture conditions, and screening in the MM will likely help us to understand the molecular mechanisms behind bacterial persisters.

The MM has also been used to study more broadly the response of bacteria to antibiotics. The device with back-channels (Fig 2.3A) was used to rapidly load cells into the device for fast antibiotic susceptibility testing (~30 min) of clinical samples[183], by directly visualizing growth or death of the bacteria during antibiotic exposure through microscopy. A study looked at the accumulation of the antibiotic ofloxacin inside *E. coli* in the MM and has shown that stationary phase cells appeared to absorb the antibiotic more slowly than exponentially growing cells[184].

2.5.7 Synthetic biology

It has become increasingly clear that cellular circuits must contend with stochastic gene expression and that this noise can have an important impact. Therefore, it is valuable to have the ability to quantify such variability for the engineering of cells for synthetic biology applications. Indeed, microfluidic devices have been instrumental in the development of synthetic gene circuits with dynamic properties[94,96,98,185,186]. The use of the MM and insights from theory of stochastic gene expression enabled the re-engineering of the repressilator - the iconic synthetic oscillator that helped kick-start the field of synthetic biology—to achieve a precision that approaches natural oscillators[67,126]. The MM was instrumental in enabling the precise characterization of the oscillators, identifying factors that disrupted oscillations, characterizing redesigned iterations of the circuit, and subsequent screening of pooled libraries. While a handful of studies have used the MM to evaluate[187,188] or control[189] synthetic gene circuits, the broader use of the MM throughout the design process could lead to a new generation of precise and robust synthetic circuits.

2.6 Discussion

Single-cell microfluidic platforms have facilitated important discoveries in a variety of fields in biology by enabling the quantification of dynamic and heterogenous processes. Recent technical developments of the MM, including the ability to phenotype or screen pooled libraries based on their dynamics, achieve better control over the growth conditions, and to culture additional organisms should continue to expand the applications of these devices to new fields. Further developments could facilitate the study of species-species interactions, as has been done in a few studies[98,190]. The majority of studies using the MM have focused on *E. coli* and *B. subtilis*,

and applications of the device to other organisms (e.g., microbes important in the clinic or in the gut microbiota) would broaden its scope. Outside the microbial realm, two studies so far have used the device with non-adherent mammalian cells[191,192]. More studies could shed light on dynamic and heterogeneous processes, such as phenotypic resistance to cancer treatment and the differentiation of hematopoietic stem cells[193–195]. Adaptation of the phenotyping and screening platforms to mammalian cells could provide an alternative to the single-cell screening techniques that have been developed[196,197].

Future studies using the MM will likely continue to advance studies of the heterogeneous processes discussed above. By showcasing discoveries in diverse fields, we hope to inspire the readers to implement such devices to explore questions in new fields and expand their possible applications. For example, the timing of other epigenetic processes in bacteria, such as prions[198,199], could be elucidated. While many studies have quantified the heterogeneity in protein production, few studies have examined how the degradation of proteins can create heterogeneity[173,200]. Although most bacteria in nature are in stationary phase[201], the majority of studies have focused on exponentially-growing bacteria. The technical developments of the MM enabling the observation of cells in different growth phases could fill this gap in the literature and generate insights into the stationary phase. Adopting the MM setup has become increasingly accessible, with molds available through different companies, detailed protocols published, and open-source data analysis software now available. Ultimately, because these microfluidic devices provide a new quantitative way to look at cells, they have the potential to continue to contribute to discoveries in diverse areas in biology.

CHAPTER 3

METABOLIC TIME-SHARING IN CLONAL MICROBIAL POPULATIONS

3.1 Introduction

Tracking single cells over time is a powerful method of characterizing dynamic cellular phenotypes, including circuit-dictated changes in gene expression. However, exploring cooperative population-level behaviour or survival strategies requires further investigation using bulk population measurements. As discussed in Sections 1.3 and 2.5.5, one example of a collaborative behaviour occurs in *B. subtilis* populations which split into distinct but cooperative subpopulations to prevent the buildup of toxic metabolic by-products[56]. In this case, single-cell studies alone were insufficient for investigating DOL, and the observation of entire microbial populations was necessary to capture these complex behaviours.

In this chapter, we show a circuit that similarly induces dynamic switching between cooperative metabolic states in an isogenic *E. coli* strain. This circuit integrates the repressilator with CRISPRi to carry out metabolic time-sharing by oscillating between distinct amino acid production states. When circuit behaviour is not synchronized between cells, the population is divided between different auxotrophy states and is able to cross-feed the required amino acids to sustain population survival (Fig 3.1). Although oscillations in gene expression occur within each individual cell, cooperative cross-feeding behaviours can only be observed at the population level. In this chapter, we begin by demonstrating the construction and characterization of a modular circuit that may be adapted for widespread DOL applications. We further combine single-cell and bulk population measurements to provide preliminary results suggesting that this circuit can give rise to obligate cross-feeding interactions within an *E. coli* population. Finally, we investigate the fitness of isogenic time-sharing populations capable of cross-feeding essential amino acids and draw comparisons to that of heterogeneous co-cultures.

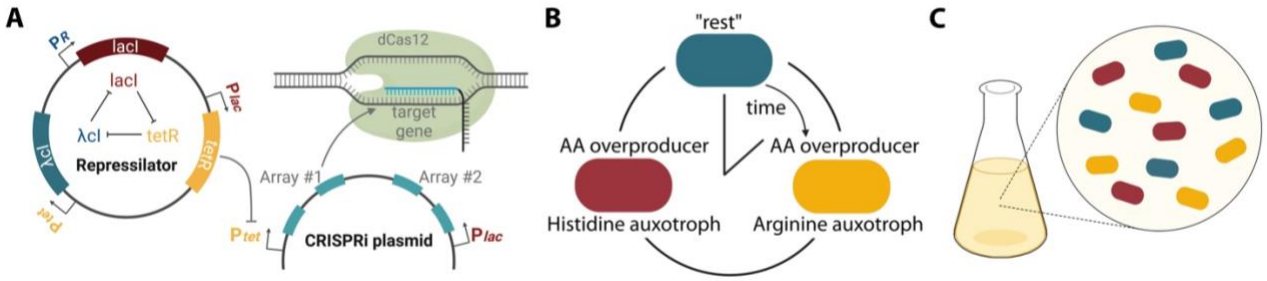

Figure 3.1 Coupling the repressilator with CRISPRi for metabolic time-sharing. **(A)** When co-expressed with the repressilator circuit, CRISPR arrays placed under control of repressilator-encoded promoters will oscillate according to the behaviour of the repressilator. The resultant crRNAs may then form a complex with dCas12 and facilitate dynamic changes in gene expression. **(B)** Each cell alternates between three distinct metabolic states with different amino acid production capabilities. **(C)** If the repressilator is unsynchronized between members of an isogenic population, approximately one third of the cells occupies each state at any given time, enabling amino acid cross-feeding between cells with different auxotrophies.

3.2 Validating the function of CRISPRi circuit components

To assemble our synthetic circuit, we first validated that we could achieve strong, sustained target gene repression using CRISPRi. Investigating static gene repression phenotypes enabled the characterization of individual circuit components prior to the introduction of dynamics into the system.

3.2.1 Tuning dCas12 expression levels impacts gene silencing efficiency

Although dCas12-related toxicity has not yet been reported in *E. coli*[72], we sought to confirm this by investigating the consequences of varying dCas12 expression levels on both gene repression efficiency, and on host cell fitness. Placing dCas12 under the control of the arabinose-inducible promoter, P_{araBAD}, enabled the tuning of its expression level. This was done by supplementing the culture medium with either increasing arabinose concentrations to proportionally increase dCas12 expression, or with 2% glucose to actively repress P_{araBAD} via catabolite repression[202]. Gene repression efficiency was investigated by co-expressing the tunable dCas12 cassette with a previously validated crRNA[203] for silencing the mVenus fluorescence gene, such that repression efficiency was determined by measuring the loss of fluorescence in single cells. However, leaky dCas12 expression was observed in both the presence and absence of glucose (Fig 3.2A). Additionally, noisy and incomplete mVenus repression was observed upon the addition

of increasing arabinose concentrations to the culture media, with no correlation between arabinose concentration and mVenus expression level.

To achieve consistent and efficient mVenus repression, we instead placed dCas12 under the control of a synthetic constitutive promoter[204]. In contrast to the inducible dCas12, constitutive expression yielded strong and homogenous mVenus repression (Fig 3.2B). This constitutive dCas12 expression cassette was therefore used for all subsequent experiments.

As the motivation for implementing metabolic time-sharing is reducing the metabolic burden placed on host cells, the circuit components were further evaluated for their effect on host growth rate. The growth of strains expressing different circuit components were monitored in minimal media over 48 hours. Comparison of calculated doubling times revealed no significant differences between that of the wildtype host and strains expressing either the constitutive dCas12 cassette alone or alongside the repressilator (Fig 3.2C). These results suggest that expression of our metabolic time-sharing circuit does not significantly impact host cell growth rate, and indicate its potential viability as a means of controlling gene expression dynamics.

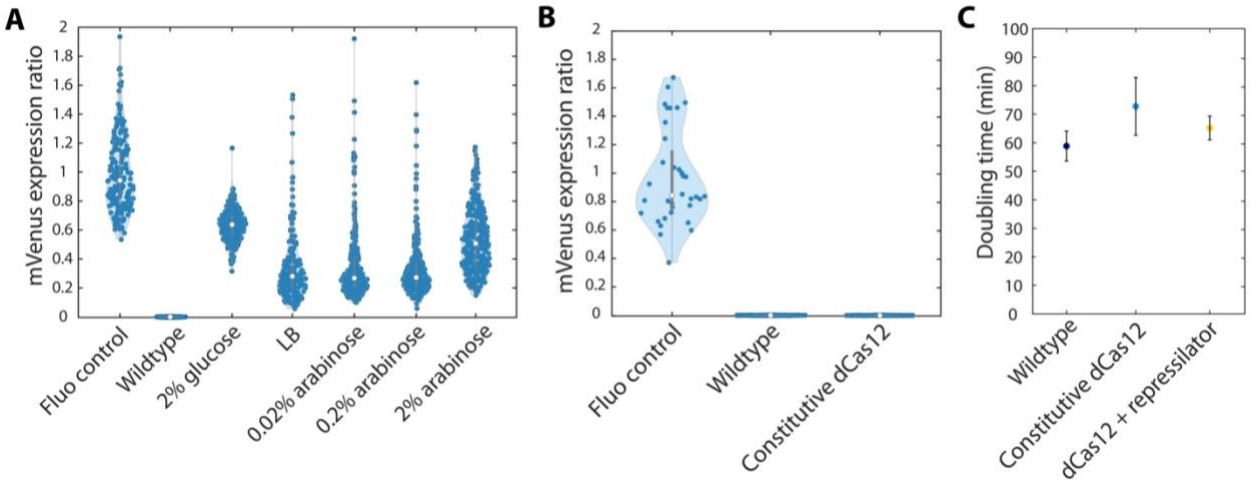

Figure 3.2 dCas12 expression affects the efficiency of mVenus silencing. Ratio of mVenus expression in single cells with varying dCas12 induction levels compared to a fluorescence control that constitutively expresses mVenus. All single-cell fluorescence values were normalized to eliminate wildtype autofluorescence prior to comparison. **(A)** Tuning arabinose-inducible dCas12 expression levels by adding increasing concentrations of arabinose or glucose to the culture medium was imprecise, and all induction conditions yielded incomplete gene silencing. (Fluo control: n=190; Wildtype: n=223; 2% glucose: n=262; LB: n=202; 0.02% arabinose: n=250; 0.2% arabinose: n=269; 2% arabinose: n=325). All repression conditions exhibited significant differences from both the wildtype and fluorescent controls (one-way ANOVA, LSD *post hoc* test $p<0.05$). **(B)** Robust silencing of mVenus using a constitutive dCas12. (Fluo control: n=37; Wildtype: n=187; Constitutive dCas12: n=111). The repression condition exhibited a significant difference from the fluorescent control (one-way ANOVA, LSD *post hoc* test $p<0.05$), but not from the wildtype. **(C)** The doubling times of cultures constitutively expressing dCas12, either alone or alongside the repressilator, compared to the wildtype host background strain. No significant differences were detected between any sample doubling times (two-sample t-test, $p>0.05$).

3.2.2 Gene silencing is robust to changes in crRNA sequence and regulatory elements

Strong target gene repression can be achieved through design and selection of optimal crRNA sequences. Here, crRNAs were selected using the methods described in Section 5.2 for their proximity to the transcription start site, as well as their lack of sequence self-complementarity and off-target matches within the genome. To demonstrate that these selection criteria can yield several different crRNA sequences, each capable of repressing target gene expression with similar efficiency, we targeted the mVenus fluorescent reporter as proof-of-principle. Two different crRNAs were selected that bind to different regions within the first third of the mVenus coding

sequence, and their ability to repress mVenus expression was compared to that of a previously validated guide[203]. Single-cell fluorescence measurements (described in Section 5.4) revealed that robust mVenus repression was achieved with each of the three crRNA sequences tested, and that no significant difference in crRNA efficacy was observed between the three evaluated sequences (Fig 3.3A). These results are consistent with previous observations that targeting regions early in the coding sequence yield strong gene repression.

To integrate CRISPRi with the repressilator, CRISPR arrays can be placed under control of different repressilator-encoded promoters, such that CRISPR array expression (and subsequent target gene repression) will oscillate according to the dynamics of the repressilator circuit. To verify that the repressilator-encoded P_{lac} and P_{tet} promoters drive sufficient crRNA expression, we expressed mVenus crRNAs under control of each repressible promoter. The drastic reduction in single-cell fluorescence intensities to undetectable levels confirmed that these promoters yielded sufficient crRNA expression to achieve tight repression of a target gene (Fig 3.3B).

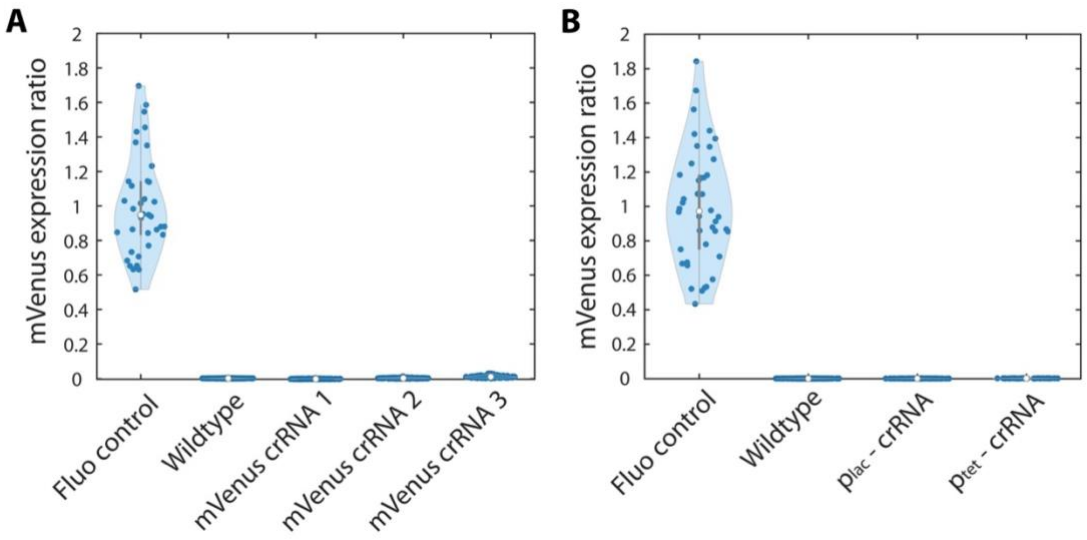

Figure 3.3 Robust mVenus silencing using different crRNA sequences and regulatory elements. Ratio of mVenus expression in single cells compared to a fluorescence control that constitutively expresses mVenus. All single-cell fluorescence values were normalized to eliminate wildtype autofluorescence prior to comparison. **(A)** Strong repression of mVenus using multiple crRNAs binding to different sequences within the mVenus coding sequence. (Fluo control: n=38; Wildtype: n=221; mVenus crRNA 1: n=185; mVenus crRNA 2: n=178; mVenus crRNA 3: n=106). **(B)** Expressing crRNAs under control of repressilator-encoded promoters yields strong target gene repression. (Fluo control: n=42; Wildtype: n=190; p_{lac}-crRNA: n=87; p_{tet}-crRNA: n=45). All samples exhibited significant differences from the fluorescent control (one-way ANOVA, LSD *post hoc* test $p<0.05$), but no significant differences were observed between the wildtype and repression conditions.

3.2.3 Workflow for modular assembly of CRISPR arrays

While expression of a single crRNA is sufficient for robust repression of a single target gene, CRISPR arrays can encode several spacers for multiplexed gene repression[71]. This is ideal for the creation of complex phenotypes, as genes in different metabolic pathways can be simultaneously perturbed. Here, we aim to engineer cells that cycle between distinct states, each characterized by the simultaneous inability to produce one amino acid and while overexpressing others. This is achieved through oscillating expression of different CRISPR arrays, which each encode two spacers: one for silencing a key amino acid biosynthetic gene, and a second for simultaneous targeting of a gene demonstrated to cause an amino acid overproduction phenotype[15].

However, the abundance of repetitive sequences inherent in the CRISPR array structure poses a challenge for array construction. To circumvent this, we adapted a previously described Golden Gate-based method for the modular assembly of spacer-repeat subunits into CRISPR arrays[70]. This method places Golden Gate-compatible cut sites within the 6-7 base pairs that are removed from the 3' end of each spacer during crRNA processing, and are therefore not necessary for targeting[70]. Designing compatible overhang sequences in the 3' end of each spacer enables the seamless assembly of multiple spacer-repeat subunits into a CRISPR array (Fig 3.4A).

To efficiently screen for successful insertion of two CRISPR arrays into a destination vector, we employed a fluorescent dropout system. We designed gBlock sequences (IDT) for assembly of a destination vector expressing two Green Fluorescence Proteins (GFPs), each under control of a different repressilator-encoded promoter. In parallel, we designed and amplified individual repeat-spacer subunits to comprise the CRISPR arrays, each flanked by complementary Golden Gate-compatible restriction sites. During successful assembly, each fluorescence gene was excised from the vector and replaced with assembled CRISPR arrays under the control of repressilator-encoded promoters (Fig 3.4B). This enabled rapid identification of successfully assembled plasmids by looking for a loss of fluorescence. Employing this method, we were able to efficiently construct several plasmids expressing CRISPR arrays with distinct spacer combinations.

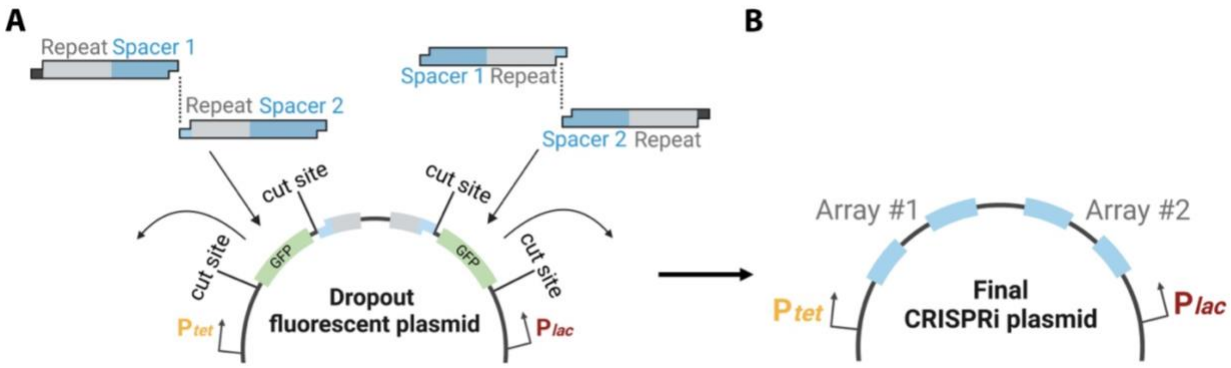

Figure 3.4 Schematic of CRISPR array cloning strategy. **(A)** Repeat-spacer subunits with compatible Type IIS restriction sites are assembled into CRISPR arrays using Golden Gate assembly. Compatible restriction sites that flank fluorescence genes in the destination plasmid facilitate the insertion of CRISPR arrays into the plasmid via Golden Gate assembly. **(B)** Successful assemblies will encode two CRISPR arrays in the place of the fluorescence genes, and can therefore be identified by screening for loss of fluorescence.

3.3 Introducing amino acid auxotrophy phenotypes through silencing of biosynthetic genes

Previous studies have demonstrated successful engineering of cross-feeding interactions within synthetic microbial consortia in *S. cerevisiae*[31] and *E. coli*[15,42], among other prokaryotes[205]. The stability of these interactions can be maintained when essential nutrients (such as amino acids) are being traded, as the survival of each member of the consortia relies on its ability to receive the desired nutrients from interacting partners. In particular, two-strain consortia consisting of histidine and arginine auxotrophs have been shown to efficiently exchange these amino acids, in some cases drastically improving the fitness of the co-culture compared to a wildtype monoculture[15].

Here, we emulate similar obligate cross-feeding interactions within a clonal *E. coli* population by oscillating between distinct amino acid auxotrophy states over time at the single-cell level. Cells occupying different states at any given time may therefore engage in reciprocal transfer of amino acids. As proof-of-principle, we engineered cells that alternate between histidine and arginine auxotrophies, motivated by a previous study demonstrating the robustness of histidine-arginine cross-feeding pairs[15]. These auxotrophic phenotypes were generated via CRISPRi-mediated silencing of key biosynthetic genes for each amino acid.

To verify whether these crRNAs were capable of creating the desired auxotrophic phenotypes, we first constructed strains expressing only the CRISPRi circuit components to induce sustained auxotrophy for a single amino acid. Two different crRNAs targeting the *hisD* or *argH* genes were evaluated for their abilities to induce histidine or arginine auxotrophy, respectively, when co-expressed with dCas12 in host cells. The growth of these strains, which lacked the repressilator for dynamic state-switching, was monitored in minimal media over a 45-hour growth period, recording population optical density (OD) at 5-minute intervals throughout (Fig 3.5A). When the culture medium lacked amino acids, auxotrophs were expected to exhibit no growth for the duration of the experiment. Conversely, providing the required amino acid by supplementing the culture medium with 100 μM of arginine or histidine was expected to restore the growth of these auxotrophs.

As expected, three of the four auxotrophs supplemented with their respective required amino acid displayed statistically similar doubling times to that of the control strain (Fig 3.5B), with only a slightly lengthened lag phase before entry into exponential growth. Interestingly, one auxotroph exhibited a significantly reduced doubling time compared to the prototrophic control when supplemented with arginine (Fig 3.5B). This may be explained by exceptionally robust silencing of the *argH* gene by this crRNA variant, causing a complete reduction in the burden associated with arginine synthesis.

In contrast, each auxotroph not supplemented with their required amino acid exhibited significantly longer lag times before entering exponential growth, ranging from 12.5 to 25 hours for different strains (Fig 3.5A). This apparent prolonged inability to grow under minimal nutrient conditions could suggest that these strains are in fact auxotrophic for their respective amino acids. However, the eventual transition into exponential growth puts this into question, prompting further investigation into this phenomenon.

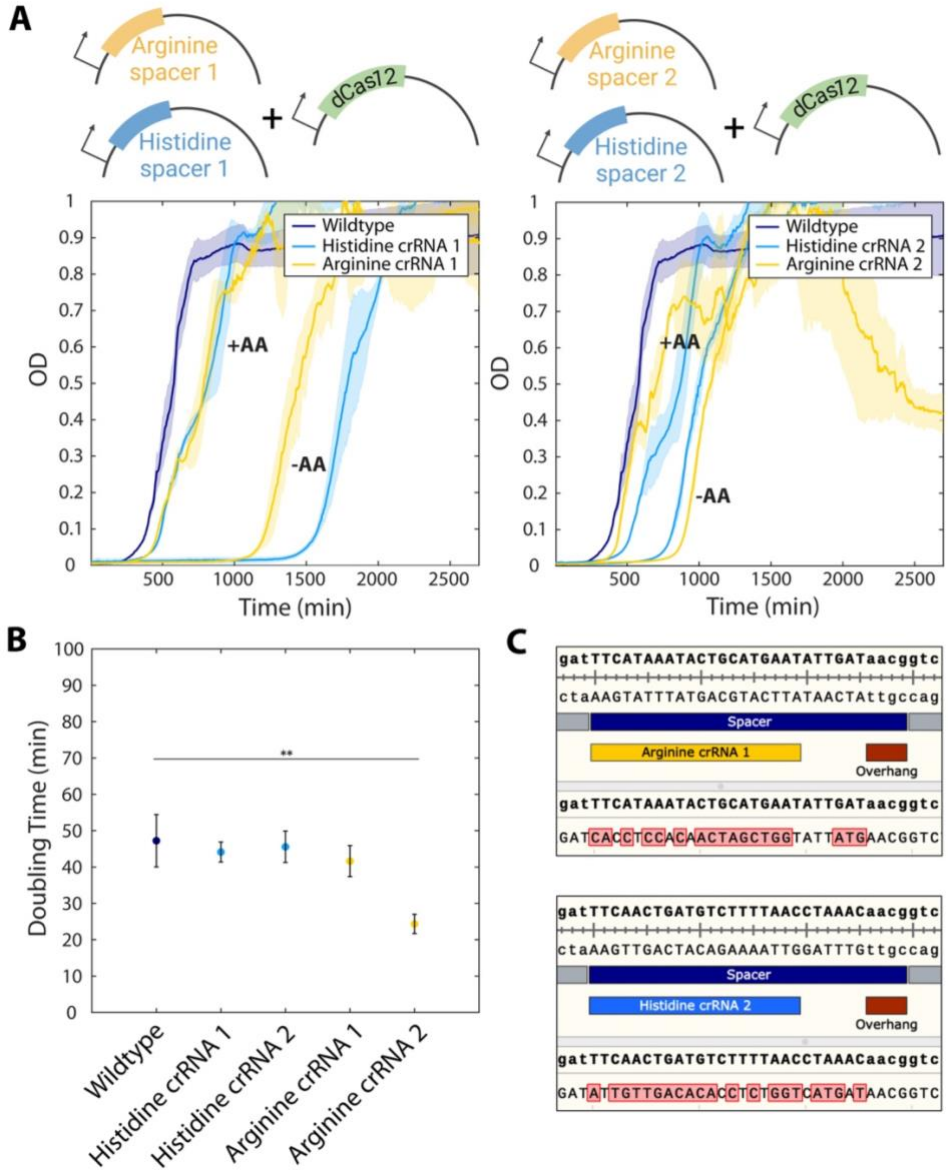

Figure 3.5 Induction of amino acid auxotrophies by silencing biosynthetic genes. **(A)** Growth of cells targeting histidine or arginine biosynthetic genes with two different crRNAs compared to the wildtype background strain in minimal media in the presence (+AA) or absence (-AA) of the required amino acid. OD measurements were taken 5 minutes apart throughout a 45-hour experiment. Shaded areas represent the standard deviation of three replicates. **(B)** Doubling times of the wildtype and auxotrophs supplemented with either arginine or histidine (+AA) to relieve the auxotrophic phenotype. An asterisk indicates a significant difference between samples (two-sample t-test, $p<0.05$). Error bars denote the standard deviation between three replicates. **(C)** Sanger sequencing of escape mutants identified at the end of the 45-hour growth experiment depicted in (A).

3.3.1 Growth of "auxotrophic" strains is likely due to the presence of escape mutants

To investigate the unexpected observation that auxotrophic strains were able to grow in the absence of amino acids after prolonged lag times, we harvested these auxotrophic cultures at the end of a 45-hour growth experiment. Sequencing of extracted plasmids revealed extensive mutations in two of the four tested crRNA sequences (Fig 3.5C). These mutations, which reduce complementarity between the crRNA and its target, impede target gene repression, therefore eliminating the auxotrophy phenotype. The uniformity in lag time between three biological replicates of each strain suggests that these "escape mutants" were present in the parent population, rather than having been individually acquired throughout the 45-hour growth experiment. As these mutants were not identified during initial Sanger sequencing of the parent population, they were likely present at very low frequencies but, as prototrophs, were selected for under the amino acid-deficient experimental conditions.

The two remaining crRNA sequences were unaffected, and sequencing additionally revealed no mutations in the dCas12 gene in any of the four tested strains. We hypothesize that these remaining two strains were likely also mutants that have acquired undetected mutations in either the target gene or another complementary region of the genome, eliminating the auxotrophic phenotype to enable growth in the absence of amino acids.

In the context of cross-feeding experiments, wherein individuals exhibiting different amino acid auxotrophies cross-feed these required amino acids among one another, rare escape mutants incur the added burden of synthesizing an additional amino acid, and should no longer be selected for. We hypothesized that the frequency of such mutants may be further reduced by co-expressing two crRNAs targeting amino acid biosynthetic genes, as the probability of acquiring mutations in both crRNA sequences is greatly reduced. To verify this, we constructed a strain expressing two CRISPR arrays (each encoding a crRNA for either arginine or histidine auxotrophy, as well as a crRNA for amino acid overproduction) in both the presence and absence of the repressilator. After pre-culturing these strains in minimal media supplemented with 100 μM of arginine and histidine, we diluted each culture to an OD of 0.005 in minimal media lacking amino acids. Upon overnight

culturing, no visible growth was observed in our "double auxotrophic" strain expressing both CRISPR arrays in the absence of the repressilator, validating that co-expression of two crRNAs can induce a sustained auxotrophic phenotype (Table 3.1). Conversely, we observed growth in our control, as well as our "time-sharing" strain expressing both CRISPR arrays and the repressilator plasmid (Table 3.1). These preliminary data also suggest that the repressilator can induce dynamic switching between alternate auxotrophic states at the single-cell level, thereby fostering reciprocal cross-feeding between cells of a population.

Table 3.1 Growth of auxotrophs in the presence and absence of the repressilator

Strain	Growth	OD after 16 h growth at 37°C
Control (expressing dCas12 only)	+	1.904
Double auxotroph	–	0.006
Time-sharing	+	0.65

3.4 Visualizing dynamic state-switching

Efficient cross-feeding between members of a time-sharing population relies on single-cell oscillations in gene expression. Oscillations may be verified in individual cells using the "triple-reporter repressilator," which encodes three different fluorescence reporters (each under the control of a different repressilator-encoded promoter) alongside the classic circuit[206]. Oscillations may therefore be visualized as out-of-phase expression of these mVenus, CFP and mCherry reporter genes. To confirm that our time-sharing strains exhibit single-cell oscillations, we co-expressed our CRISPRi circuit that induces alternate amino acid production states with the triple-reporter repressilator and analyzed single-cell fluorescence. Cells were observed on agarose pads, and static mCherry, mVenus, and CFP intensity measurements were obtained for each cell and plotted on a 3D scatterplot (Fig 3.6). Here, we observed the trend that single-cell fluorescence fell along one of the three axes, although variability in fluorescence intensity was observed. This suggests that one fluorophore primarily dominates the system within each cell at any given time, which is consistent with out-of-phase oscillations. As the dynamics of CRISPR array expression in our system are also

dictated by the repressilator, cells expressing different fluorescent proteins are indicative of cells occupying distinct metabolic states.

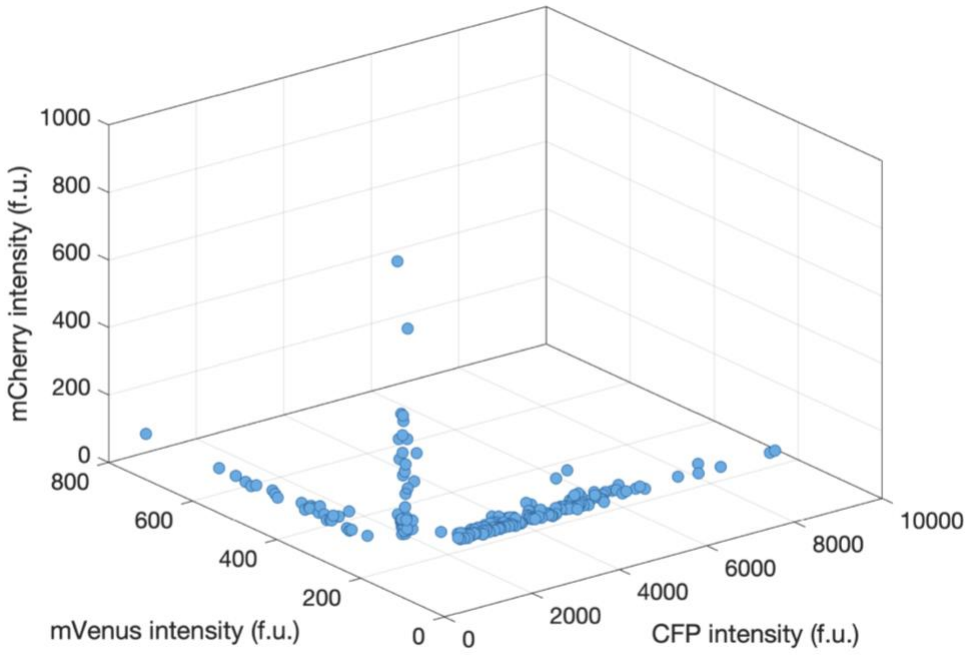

Figure 3.6 Using the triple reporter repressilator to observe state switching. Single-cell mCherry, mVenus, and CFP intensities in fluorescence units (f.u.). The buffer preventing fluorescence intensity from reaching zero along any axis represents baseline autofluorescence in that channel. Each dot represents a single cell (n=222).

3.5 Implications of metabolic time-sharing on population fitness

While single-cell measurements are ideal for monitoring dynamic processes in individual cells over time, alternative methods are necessary to evaluate cooperative population-level behaviours such as reciprocal cross-feeding. In an exponentially-growing isogenic population expressing our time-sharing circuit, the repressilator is unsynchronized between individuals, thus creating distinct subpopulations of cells exhibiting different amino acid auxotrophy and overproduction phenotypes. Culturing in minimal media lacking amino acids therefore necessitates amino acid cross-feeding between subpopulations. Similarly, cross-feeding can be achieved in heterogeneous *E. coli* consortia composed of distinct strains of metabolic specialists. Here, we created heterogeneous co-cultures by inoculating minimal media with two distinct auxotrophic

strains (each expressing CRISPRi machinery for sustained silencing of either an arginine or histidine biosynthetic gene) at identical initial densities. Segregating different amino acid auxotrophies into separate strains has been demonstrated to foster reciprocal cross-feeding[15,42,205], but such heterogeneous consortia are susceptible to instability and competition between strains. To evaluate the utility of metabolic time-sharing, we compared the fitness of a time-sharing strain with that of a heterogeneous co-culture, each capable of cross-feeding essential amino acids in an environment devoid of the required nutrients (Fig 3.7). The fitness of these cross-feeding cultures were additionally compared with that of a "double auxotroph" unable to synthesize arginine or histidine, as well as a prototrophic control strain expressing only dCas12.

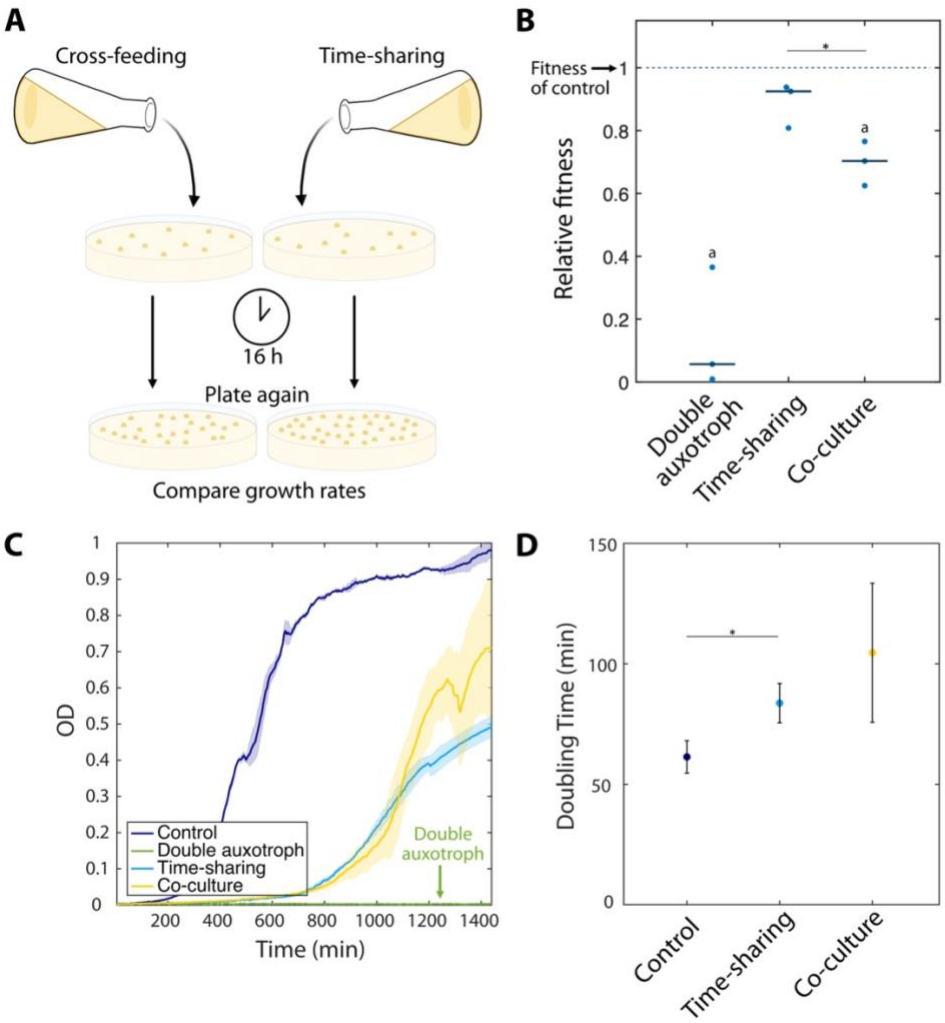

Figure 3.7 Fitness and growth of monocultures and co-cultures cross-feeding amino acids. (A) Schematic of the Viable Plate Count method used here to determine the fitnesses of cross-feeding co-cultures and time-sharing monocultures. **(B)** Fitness of cultures relative to a control strain expressing only dCas12 during 16 hours in minimal media lacking amino acids (n=3 experimental replicates; horizontal lines indicate the mean). The letter a indicates significant difference from a relative fitness of 1 (one-sample t-test, $p < 0.05$). **(C)** Growth of a prototrophic control, arginine and histidine double auxotroph, time-sharing strain, and cross-feeding co-culture in minimal media lacking amino acids. OD measurements were taken 5 minutes apart throughout a 24-hour experiment. Shaded areas represent the standard deviation of three replicates. **(D)** Doubling times of cultures in minimal media devoid of amino acids, derived from the growth rates observed in (B). Error bars denote the standard deviation between three replicates. An asterisk indicates a significant difference between two samples (two-sample t-test, $p<0.05$).

Firstly, the growth of each auxotrophic or cross-feeding culture was investigated using the Viable Plate Count (VPC) method, and the fitness of each was determined relative to the prototrophic control. Aliquots of cultures diluted to an initial OD of 0.005 were spread onto agar plates at the beginning and end of a 16-hour growth period, and the observed change in Colony Forming Units (CFU) per mL was used to estimate population growth rates (Figure 3.7A). The fitness of each culture relative to a prototrophic control strain was thus determined using the ratio of growth rates. Growth experiments revealed that the fitness's of both the double auxotroph and the heterogeneous co-culture were significantly lower than that of the control strain. Although both cross-feeding cultures reached a lower maximum OD than that of the control, no statistical difference was found between the fitness's of our time-sharing strain and the control. This observation provides preliminary evidence that metabolic time-sharing may be used to generate robust cross-feeding interactions capable of sustaining population growth (Fig 3.7B). Interestingly, the fitness of our time-sharing strain was found to be significantly higher than that of the heterogeneous co-culture, indicating that time-sharing may be a viable alternative to employing co-cultures for DOL.

While VPCs are valuable for providing overall population growth rates, such end-point measurements are unable to capture dynamic growth characteristics. For this reason, we additionally monitored the growth of both cross-feeding cultures and controls in minimal media devoid of amino acids, recording OD measurements at 5-minute intervals over a 24-hour observation period. Such time-lapse data enabled the construction of growth curves for each culture, displaying characteristics such as the lag time prior to exponential phase. Similar to observations from VPC experiments, both cross-feeding cultures reached a lower maximum OD than the control (Fig 3.7C). Further, the double auxotrophic strain exhibited no calculable growth over the duration of the experiment while amino acid cross-feeding enabled the growth of both the time-sharing strain and heterogeneous co-culture in an environment devoid of amino acids (Fig 3.7C). Doubling time estimations obtained using the observed slope of the log(OD) revealed that our time-sharing strain exhibited a significantly higher doubling time (and therefore slower growth rate) compared to a prototrophic control (Fig 3.7D). Though our time-sharing strain similarly exhibited a lower fitness than the control in the VPC experiments, the significance of this difference was not discerned by the VPC technique. However, no significant differences were observed

between the doubling times of the time-sharing population and heterogeneous co-culture, suggesting that our time-sharing method is comparable to traditional methods of engineering obligate cross-feeding interactions. These preliminary results provide evidence that engineered metabolic time-sharing has potential as a means of invoking cooperative population-level processes.

CHAPTER 4

CONCLUSIONS AND FUTURE DIRECTIONS

In this thesis, we present a versatile platform for generating dynamic shifts between distinct metabolic states in single *E. coli* cells using a hybrid circuit employing elements of CRISPR interference and the repressilator. The resultant heterogeneity between individual cells harbouring this "metabolic time-sharing" circuit enables cooperative population-level behaviours, such as reciprocal nutrient cross-feeding. In Chapter 2, we discussed the advantages and applications of single-cell monitoring and imaging techniques. Here, we highlighted the prominent "mother machine" microfluidic platform and related devices, which facilitate the tracking of thousands of individual cells in parallel under precisely controlled growth conditions. In Chapter 3, we employed a combination of endpoint and time-lapse techniques to characterize the phenotypes of individual cells, as well as whole populations, exhibiting metabolic time-sharing.

While the classic repressilator circuit has been demonstrated to generate robust oscillations in reporter gene expression[67], its applicability is limited to altering the expression dynamics of genes under control of the p_{lac}, p_{tet}, or p_R promoters encoded within the circuit. The repressilator alone is therefore ill-suited for orchestrating shifts between metabolic states, as extensive genetic modification would be required to place native metabolic genes under control of repressilator-encoded promoters. Previous work has demonstrated oscillator circuits that utilize CRISPRi machinery to recapitulate the topology of the repressilator[203,207]. Rather than encoding three repressor proteins, these circuit variations encode three crRNAs, which each repress the expression of the subsequent crRNA in the circuit. Conversely, we express the original repressilator circuit in parallel with CRISPRi machinery, such that the repressilator dictates the dynamics of CRISPRi-induced gene repression. Expressing multiple CRISPR arrays under the control of different repressilator-encoded promoters enables switching between distinct gene expression states. To our knowledge, this is the first synthetic oscillator circuit that couples host cell metabolism with CRISPRi to alternate between complementary metabolic states.

As proof-of-principle that this platform may be used to engineer cooperative behaviours, we adapted our metabolic time-sharing circuit to oscillate between distinct amino acid production states. Amino acid auxotrophies induced in one metabolic state are complemented by others, such that when a population of time-sharing cells is cultured, cells occupying different states at any given time are able to reciprocally cross-feed the required amino acids. This distribution of isogenic cells between three distinct states was visualized through the out-of-phase expression of three fluorophores encoded in the triple reporter repressilator.

Time-trace data recording the OD of *E. coli* strains over a 45-hour experiment revealed the unexpected growth of histidine or arginine "auxotrophic" strains following a prolonged delay. As the cell growth medium was devoid of amino acids, this observation seemingly contradicted our hypothesis that our auxotrophic strains would only exhibit growth upon supplementation of the culture medium with the required amino acids. Upon further investigation, we identified mutations in two of the four crRNA sequences used to induce auxotrophy at the conclusion of a growth experiment. These mutations, which were sufficient to eliminate complementarity between crRNA and target gene, were not detected in the parent culture. As the variation was small between replicates monitored throughout the experiment, it is unlikely that these mutations were independently acquired in each replicate throughout the experiment. Rather, this data suggests the presence of low frequency "escape mutants" in the parent culture which, as the sole prototrophs in the culture, were selected for and became enriched over time under conditions lacking extracellular amino acids. The enrichment of these mutants in the population over time was captured using kinetic OD measurements, which track dynamic growth characteristics. To the contrary, endpoint OD measurements taken at the conclusion of the experiment would have solely reported growth of the "auxotrophic" strains, without capturing the initial prolonged lag phase that prompted further investigation.

As these escape mutants are selected against under time-sharing conditions, due to the burden of synthesizing an additional amino acid compared to their cross-feeding counterparts, we hypothesize that escape mutants do not impact the observed growth and fitness of time-sharing populations. However, the prevalence of such mutants may be reduced in future work by employing an additional crRNA targeting each amino acid biosynthetic gene for silencing, as the likelihood

of cells within the parent population acquiring mutations in both crRNAs is greatly reduced. The efficacy of using two crRNAs was observed in our "double auxotroph" strain, which simultaneously expressed crRNAs targeting arginine and histidine biosynthetic genes, and consistently displayed no calculable growth during experiments. As the "no growth" phenotype relies on only one of these crRNAs to be functional, the likelihood of aberrant growth in this strain is greatly diminished.

Employing alternative methods to measure population fitness yielded similar trends, although differences in statistical significance were detected. The results of VPC experiments suggest that our time-sharing strain alternating between amino acid auxotrophies exhibits higher fitness in minimal media than a heterogeneous co-culture of auxotrophic strains. However, measurements taken from time-lapse growth experiments indicate no significant fitness differences between time-sharing strains and co-cultures that cross-feed amino acids. These observations highlight the benefits of time-lapse tools for recording dynamic behaviours, such as population growth. While VPCs have been considered the "gold standard" for measuring population fitness[208], this technique relies on endpoint measurements which mask defining growth characteristics, and is laborious, as it relies on the manual counting of CFUs. Furthermore, these results are inconsistent with one study that observed approximately a 20% increase in fitness of an arginine-histidine cross-feeding co-culture compared to a wildtype control, although differences in the employed growth conditions may explain this disparity[15]. As this study primarily used VPC methods to estimate community fitness, the observed discrepancy may also be attributed to low countable numbers of CFUs that reduce the power of the technique. Alternatively, the expression of CRISPRi machinery in our system, which was not employed in the previous study may be responsible for this inconsistency, although further exploration of the burden associated with CRISPRi would be required to confirm this. Nevertheless, we can conclude that using our metabolic time-sharing system to engineer cooperative behaviours in *E. coli* populations provides a comparable fitness benefit as segregating the same cooperative interactions into heterogeneous co-cultures.

A drawback of using multi-strain consortia for cross-feeding and other cooperative processes is the instability associated with co-culturing multiple strains within the same environment[23,47,48]. Conversely, the metabolic time-sharing method presented here is executed

within a single, isogenic population, thereby eliminating this disadvantage. To investigate the robustness of time-sharing populations, we suggest that the following experiment be included in future work. The metabolic time-sharing population should be adapted, such that each cell will alternate between being resistant to two distinct environmental stressors, such as the bactericidal antibiotics ampicillin and kanamycin. In parallel, a co-culture should be inoculated with two strains at identical starting densities: one resistant to ampicillin and the other resistant to kanamycin. Challenging both the co-culture and time-sharing population with one of the two stressors (i.e. ampicillin) is expected to create an initial population bottleneck in both cultures, as all cells not resistant to ampicillin at the time of exposure should be eliminated. However, the time-sharing population is expected to regenerate its diversity over time, as each individual cell carries the capacity to occupy both resistance states. Conversely, the co-culture should be unable to recover the ampicillin resistance phenotype, and would therefore have lost half of its diversity. This experiment would highlight the robustness of metabolic time-sharing in the face of environmental changes.

The presented metabolic time-sharing platform has ideal applications in the biotechnology industry for the synthesis of valuable compounds and chemicals with complex biosynthetic pathways. We suggest that future work focus on the adaptation of our metabolic time-sharing circuit to the alternating expression of sequential pathway modules for compound production. Synthesis of the pigment violacein would be an ideal proof-of-concept to demonstrate the utility of this method for progressing through biological pathways, as its synthesis pathway has been extensively characterized, and the purple colour of the end product enables yield estimations through colorimetric assays[209,210]. Additionally, it has been reported that simultaneous expression of the entire violacein biosynthetic pathway imposes a metabolic burden on the host[45]. Adopting a metabolic time-sharing approach is therefore anticipated to lower the burden placed on host cells, as only one pathway module would be expressed at any given time, although this would require future work to validate. Potential migration of this circuit into yeast could expand the range of value-added compounds that may be synthesized using this method, but would require several adaptations. These include altering the CRISPRi setup to use a dCas enzyme fused to a Krüppel-associated box (KRAB) domain for tight target gene repression[211], reconstruction of the

repressilator to include eukaryotic transcriptional repressors, and ensuring the ability of transcription factors to enter the nucleus.

Future directions could additionally focus on exploring the versatility of this metabolic time-sharing system. The MM microfluidic platform could be used to screen large repressilator libraries, with the aim of uncovering circuit variants with differing dynamic properties (i.e. period, amplitude). Bioproduction of specific compounds which require fixed ratios of time to be spent in each state could benefit from selecting a circuit with the ideal dynamics. Characterizing a plethora of circuits may therefore prove useful for tailoring this platform to a variety of applications.

DOL is a powerful phenomenon which has enabled natural microbial communities to cooperatively perform complex metabolic tasks. Here, we present a platform to emulate this behaviour within genetically identical *E. coli* populations and evaluate its ability to introduce obligate cross-feeding interactions into a population. To the best of our knowledge, this is the first time this fundamental property of higher organisms is engineered and harnessed but we foresee widespread applications, such as DOL to synthesize valuable compounds with increased efficiency, by providing a new paradigm for synthetic communities.

CHAPTER 5

MATERIALS AND METHODS

5.1 Plasmid construction

The plasmids described in this thesis were constructed using Gibson assembly and/or Golden Gate assembly, and are compiled in Table 5.1. Phusion high-fidelity DNA polymerase (New England Biolabs) or AccuPrime pfx DNA polymerase (Invitrogen) were used according to manufacturer specifications for PCR amplification of plasmid fragments or gBlocks (Integrated DNA Technologies). All primers and oligos were purchased from ThermoFisher Scientific. Plasmids were sequence-verified by Sanger sequencing (The Centre for Applied Genomics) or Oxford Nanopore sequencing (Plasmidsaurus). Golden Gate assemblies were performed in T4 ligase buffer (New England Biolabs), using T4 DNA ligase (New England Biolabs) and BsmBI or BsaI type IIS restriction enzymes (New England Biolabs). All plasmids were assembled in Sigma10 cells (Sigma Aldrich) treated to be either chemically competent (using Transformation and Storage Solution (TSS)) or electrocompetent, and were subsequently transformed into the desired background strain following successful assembly.

CRISPR arrays were cloned into a parent plasmid using the CRATES Golden Gate assembly method[70]. Each crRNA was designed with flanking appropriate BsmBI recognition sites and overhangs for array assembly, and purchased as a set of complementary single-stranded oligos. Oligos were annealed by mixing equimolar concentrations of each complementary single-stranded oligo in annealing buffer (10 mM Tris (pH 7.5-8.0), 1 mM EDTA (pH 8.0), 50 mM NaCl), heating to 95ºC for 5 mins, and gradually cooling down to room temperature over 1-2 hours.

Plasmids pTP115 and pTP116 were constructed through restriction cloning. BamHI and EcoRI restriction sites were placed flanking the lac and tet promoter fragments, which were ordered as sets of single-stranded complementary oligos and annealed as described above. The pTP84 vector backbone (gift of Chase Beisel[70]) was PCR amplified using primers that incorporate BamHI and EcoRI restriction sites into the amplified plasmid. The amplified plasmid and annealed

promoter sequences were digested by BamHI (New England Biolabs) and EcoRI-HF (New England Biolabs) according to manufacturer protocols. pTP115 and pTP116 were individually assembled by annealing one of the promoters into the digested backbone using T4 DNA ligase and its associated buffer (New England Biolabs).

The promoter controlling dCas12 expression was swapped with Gibson assembly, using the NEBuilder HiFi DNA assembly mix (New England Biolabs). The araBAD promoter for arabinose-inducible dCas12 expression in pTP92 was derived from pZA16mflon (gift from James Collins[212]). The constitutive promoter sequence (pJ23100) used to drive dCas12 expression in pTP118 and pTP200 was taken from the EcoFlex MoClo kit for *E. coli*[204], and its corresponding Ribosome Binding Site (RBS) was designed using the Salis Lab RBS calculator[213]. The pJ23100-RBS sequence fragment was assembled using assembly PCR[214] and assembled into the pJK506 backbone. pTP200 was similarly constructed via Gibson assembly by swapping the SC101 origin of replication for the p15A origin, derived from pJS169 (gift from Jeff Hasty).

pTP116 was generated by assembling a gBlock and kanamycin resistance cassette (derived from pTP26) into the psgRNA backbone.

Table 5.1 Plasmid list

Plasmid	Parent	Origin of Replication	Antibiotic Resistance	Genotype
pFNCpf1 GG	Gift of Chase Beisel	ColE1	Ampicillin	p_{J23119}-*dropout sfGFP*
pJS169	Gift of Jeff Hasty	p15A	Ampicillin	$p_{ara/lac}$-*lacI-ssrA*
pJK506	Gift of Pamela Silver	SC101	Chloramphenicol	$p_{tetR/tetA}$-*dCas12*, $p_{tetR/tetA}$-*tetR*, p_{A4}-*mVenus*
pLPT196		SC101	Ampicillin	Repressilator, p_{tet}-*cI* , p_{lac}-*tetR*, p_R-*lacI*
pLPT234		SC101	Ampicillin	Triple reporter repressilator, p_{tet}-*cI*, p_{lac}- *tetR*, p_R-*lacI*, p_{tet}-*mVenus*, p_{lac}- *mSCFP3,* p_R-*mKate2*
psgRNA	Gift of David Bikard	ColE1	Kanamycin	p_{J23119}-*gRNA scaffold*
pTP88	Gift of Chase Beisel	ColE1	Ampicillin	p_{J23119}-*mVenus crRNA 1*
pTP89	Gift of Chase Beisel	ColE1	Ampicillin	p_{J23119}- *mVenus crRNA 2*
pTP90	Gift of Chase Beisel	ColE1	Ampicillin	p_{J23119}- *mVenus crRNA 3*
pTP92	Gift of Pamela Silver	SC101	Chloramphenicol	p_{araBAD}-*dCas12*, p_{A4}-*mVenus*
pTP107	Gift of Chase Beisel	ColE1	Ampicillin	p_{J23119}-*hisD crRNA 1*
pTP108	Gift of Chase Beisel	ColE1	Ampicillin	p_{J23119}-*hisD crRNA 2*
pTP109	Gift of Chase Beisel	ColE1	Ampicillin	p_{J23119}-*argH crRNA 1*
pTP110	Gift of Chase Beisel	ColE1	Ampicillin	p_{J23119}-*argH crRNA 2*
pTP115	Gift of Chase Beisel	ColE1	Ampicillin	p_{lac}-*dropout sfGFP*

pTP116	Gift of Chase Beisel	ColE1	Ampicillin	p_{tet}-*dropout sfGFP*
pTP118	Gift of Pamela Silver	SC101	Chloramphenicol	p_{J23100}-*dCas12*, p_{A4}-*mVenus*
pTP119	pTP115	ColE1	Ampicillin	p_{lac}-*mVenus crRNA 1*
pTP120	pTP116	ColE1	Ampicillin	p_{tet}-*mVenus crRNA 1*
pTP125	Gift of Chase Beisel	ColE1	Ampicillin	p_{J23119}-*hisD operon crRNA 1*
pTP126	Gift of Chase Beisel	ColE1	Ampicillin	p_{J23119}-*hisD operon crRNA 2*
pTP127	Gift of Chase Beisel	ColE1	Ampicillin	p_{J23119}-*argH operon crRNA 1*
pTP128	Gift of Chase Beisel	ColE1	Ampicillin	p_{J23119}-*argH operon crRNA 2*
pTP141	pTP116	ColE1	Kanamycin	p_{tet}-*dropout sfGFP*, p_{lac}-*dropout mNeon green*
pTP162	pTP141	ColE1	Kanamycin	p_{tet}-*argH crRNA 1-mdh crRNA 1*, p_{lac}-*hisD crRNA 1, ppc crRNA 1*
pTP200	pTP118	p15A	Chloramphenicol	p_{J23100}-*dCas12*
pTP213	pTP115	ColE1	Ampicillin	p_{lac}-*his operon crRNA 1-ppc crRNA 1*
pTP214	pTP116	ColE1	Ampicillin	p_{tet}-*arg operon crRNA 1-mdh crRNA 1*
pZA16mflon	Gift of James Collins	p15A	Ampicillin	p_{araBAD}-*mf lon*

5.2 CRISPRi

All crRNAs used in this thesis are listed in Table 5.2, and were designed using the CHOPCHOP tool[215], with the exception of *mVenus* crRNA 1, which has been previously designed and validated to silence genes under control of the A4 promoter[203].

Targeted gene silencing was achieved through co-expression of one or more crRNAs with dCas12. Arabinose-inducible dCas12 cassettes were either induced overnight through the addition of 0.02%, 0.2% or 2% arabinose to the culture medium, or repressed by adding 2% glucose to the culture medium.

Table 5.2 crRNA list

crRNA	Target gene	Sequence (5' to 3')	Target region	Target strand*
mVenus crRNA 1	*mVenus*	CACCTCCACAACTAGCTGGT	Promoter	– strand
mVenus crRNA 2	*mVenus*	ACTGGAGTTGTCCCAATTCT	ORF	– strand
mVenus crRNA 3	*mVenus*	TGTCAGTGGAGAGGGTGAAG	ORF	– strand
hisD crRNA 1	*hisD*	ACCTAAACCACTTTCACGTT	Promoter	+ strand
hisD crRNA 2	*hisD*	TTCAACTGATGTCTTTTAAC	Promoter	+ strand
hisD crRNA 3	*hisD*	ACACAATCATTGACTGGAAT	ORF	– strand
hisD crRNA 4	*hisD*	CGCCTCTGAAAGCATTACCC	ORF	– strand
argH crRNA 1	*argH*	TTCATAAATACTGCATGAAT	Promoter	– strand
argH crRNA 2	*argH*	ATTGTTGACACACCTCTGGT	Promoter	– strand
argH crRNA 3	*argH*	CCCAGGCAGCAGATCAACGG	ORF	– strand
argH crRNA 4	*argH*	ATTACCGTCTGGCGGAGCAG	ORF	– strand
mdh crRNA 1	*mdh*	ACAGTAGTGCAAGCGCCTGG	ORF	– strand
ppc crRNA 2	*ppc*	CCGAGCATACTGACATTACT	ORF	– strand

*"Target strand" indicates the strand that is complementary to the crRNA

5.3 Strain preparation and culturing

The wildtype strain used was LPT370, a derivative of MG1655 (gifted by Mustafa Khammash[216]), and all strains used in this thesis are listed in Table 5.3. Strains were cultivated at 37ºC in LB media (Fisher Scientific) for propagation, or M9 minimal media (1x M9 salts (Thermo), 2 mM $MgSO_4$, 0.001 mg/mL thiamine HCl, 0.4% glucose, 0.02 mg/mL uracil, 0.1 mM $CaCl_2$) during growth experiments with the appropriate antibiotics.

Table 5.3 Strain list

Strain	Parent	Genotype	Plasmids
LPT370	MG1655	ΔaraCBAD ΔlacIZYA ΔaraE ΔaraFGH attB::lacYA177C ΔrhaSRT ΔrhaBADM	-
TP96	LPT370	ΔaraCBAD ΔlacIZYA ΔaraE ΔaraFGH attB::lacYA177C ΔrhaSRT ΔrhaBADM	pTP85
TP97	LPT370	ΔaraCBAD ΔlacIZYA ΔaraE ΔaraFGH attB::lacYA177C ΔrhaSRT ΔrhaBADM	pTP85, pTP88
TP98	LPT370	ΔaraCBAD ΔlacIZYA ΔaraE ΔaraFGH attB::lacYA177C ΔrhaSRT ΔrhaBADM	pTP85, pTP89
TP99	LPT370	ΔaraCBAD ΔlacIZYA ΔaraE ΔaraFGH attB::lacYA177C ΔrhaSRT ΔrhaBADM	pTP85, pTP90
TP101	LPT370	ΔaraCBAD ΔlacIZYA ΔaraE ΔaraFGH attB::lacYA177C ΔrhaSRT ΔrhaBADM	pTP88, pTP92
TP105	LPT370	ΔaraCBAD ΔlacIZYA ΔaraE ΔaraFGH attB::lacYA177C ΔrhaSRT ΔrhaBADM	pTP92
TP121	LPT370	ΔaraCBAD ΔlacIZYA ΔaraE ΔaraFGH attB::lacYA177C ΔrhaSRT ΔrhaBADM	pTP85, pTP119
TP122	LPT370	ΔaraCBAD ΔlacIZYA ΔaraE ΔaraFGH attB::lacYA177C ΔrhaSRT ΔrhaBADM	pTP85, pTP120
TP133	LPT370	ΔaraCBAD ΔlacIZYA ΔaraE ΔaraFGH attB::lacYA177C ΔrhaSRT ΔrhaBADM	pTP118, pTP125
TP134	LPT370	ΔaraCBAD ΔlacIZYA ΔaraE ΔaraFGH attB::lacYA177C ΔrhaSRT ΔrhaBADM	pTP118, pTP126

TP135	LPT370	ΔaraCBAD ΔlacIZYA ΔaraE ΔaraFGH attB::lacYA177C ΔrhaSRT ΔrhaBADM	pTP118, pTP127
TP136	LPT370	ΔaraCBAD ΔlacIZYA ΔaraE ΔaraFGH attB::lacYA177C ΔrhaSRT ΔrhaBADM	pTP118, pTP128
TP137	LPT370	ΔaraCBAD ΔlacIZYA ΔaraE ΔaraFGH attB::lacYA177C ΔrhaSRT ΔrhaBADM	pTP88, pTP118
TP138	LPT370	ΔaraCBAD ΔlacIZYA ΔaraE ΔaraFGH attB::lacYA177C ΔrhaSRT ΔrhaBADM	pTP118
TP201	LPT370	ΔaraCBAD ΔlacIZYA ΔaraE ΔaraFGH attB::lacYA177C ΔrhaSRT ΔrhaBADM	pTP200
TP202	LPT370	ΔaraCBAD ΔlacIZYA ΔaraE ΔaraFGH attB::lacYA177C ΔrhaSRT ΔrhaBADM	pTP200, pLPT196
TP205	LPT370	ΔaraCBAD ΔlacIZYA ΔaraE ΔaraFGH attB::lacYA177C ΔrhaSRT ΔrhaBADM	pTP162, pTP200, pLPT196
TP206	LPT370	ΔaraCBAD ΔlacIZYA ΔaraE ΔaraFGH attB::lacYA177C ΔrhaSRT ΔrhaBADM	pTP162, pTP200
TP217	LPT370	ΔaraCBAD ΔlacIZYA ΔaraE ΔaraFGH attB::lacYA177C ΔrhaSRT ΔrhaBADM	pTP200, pTP213
TP218	LPT370	ΔaraCBAD ΔlacIZYA ΔaraE ΔaraFGH attB::lacYA177C ΔrhaSRT ΔrhaBADM	pTP200, pTP214
TP221	LPT370	ΔaraCBAD ΔlacIZYA ΔaraE ΔaraFGH attB::lacYA177C ΔrhaSRT ΔrhaBADM	pTP162, pTP200, pLPT234

5.4 Single-cell fluorescence measurements

E. coli strains were grown overnight in LB medium prior to fluorescence measurements. The following morning, cultures were diluted 1:100 and grown another 2 hours at 37ºC. 1 μL of diluted culture was pipetted onto an agar pad, and cells were observed using a Zeiss Axio Observer inverted microscope. An attached LED epifluorescence illuminator (Collibri 7) was used for fluorescence excitation, and emitted fluorescence was captured with an Orca Flash 4.0 LT camera (Hamamatsu).

5.5 Growth curves

E. coli strains were pre-cultured overnight in LB media prior to growth experiments. The following morning, cultures were diluted 1:00 and grown another 2 hours at 37ºC. Diluted cultures were washed 3 times and resuspended in M9 minimal media lacking amino acids. Resuspended cultures were diluted to an OD 0.005 in M9 minimal media with or without 100 μM of arginine or histidine. Co-cultures were created by inoculating M9 minimal media with two strains at a 1:1 ratio, each at an initial OD of 0.025. 150 μL of each culture was pipetted in triplicate into a 96-well plate (Greiner Bio-One) alongside a 150 μL "blank" of M9 minimal media. OD was measured at 5-minute intervals with continuous shaking at 282 cycles per minute using a Synergy H1 microplate reader (BioTek) set to 37ºC.

5.6 VPC experiments

Prior to the VPC experiment, *E. coli* strains were streaked onto LB plates supplemented with the appropriate antibiotics, and one isolated colony of each strain was cultured overnight at 37ºC. The following morning, overnight cultures were diluted 1:50 and incubated for another 3 hours at 37ºC prior to being washed 3 times and resuspended in M9 minimal media. Resuspended cultures were diluted to an OD of 0.005 at the start of the experiment, and were grown at 37ºC for 16 hours. At the beginning (0-hour) and end (16-hour) of the experiment, 100 μL was removed from each culture for 10-fold serial dilutions. 100 μL of the 10^{-4}, 10^{-5}, and 10^{-6} dilutions were plated onto LB plates with the appropriate antibiotics at each timepoint. The number of CFUs on each plate after overnight growth at 37ºC were counted manually.

5.7 Data analysis

5.7.1 Single-cell fluorescence measurements

Cells were manually segmented and fluorescence intensity values were determined using FIJI (Fiji Is Just ImageJ). All images were concatenated before adjusting image brightness and contrast. Each cell was manually selected and the maximum pixel intensity of each cell was

recorded. To remove autofluorescence, the mean intensity of a non-fluorescent control strain was subtracted from the intensities of each individual cell. The adjusted intensity of each cell was then divided by the mean intensity of a control strain constitutively expressing mVenus (relative expression value of "1") to determine mVenus expression ratios. Violin plots were created using MATLAB (code provided by Bastian Bechtold).

5.7.2 Growth experiments

Changes in population OD over time were plotted using MATLAB (code provided by Giselle McCallum). Shaded error bars represent the standard deviation of three replicates, while the bolded lines represent the mean. Growth rate was determined by finding the slope of the linear region in a plot of log(OD) over time. Doubling time was calculated by dividing ln(2) by the determined growth rate.

5.7.3 VPC experiments

The observed change in CFU/mL was used to calculate the Malthusian parameter (M) as an estimation of population fitness (Equation 1). Relative fitness of a culture compared to a control was determined by the ratio of Malthusian parameters (Equation 2).

$$M = \frac{ln(\frac{CFU/mL\ at\ time\ t}{CFU/mL\ at\ time\ 0})}{time\ t} \quad \text{(Eqn 1)}$$

$$Rel.fitness = \frac{M(strain)}{M(control)} \quad \text{(Eqn 2)}$$

CHAPTER 7

REFERENCES

1. Bar-On, Y. M., Phillips, R. & Milo, R. The biomass distribution on Earth. *Proc. Natl. Acad. Sci. U. S. A.* **115**, 6506–6511 (2018).
2. Wright, C. J. *et al.* Microbial interactions in building of communities. *Mol. Oral Microbiol.* **28**, 83–101 (2013).
3. Cordero, O. X. & Datta, M. S. Microbial interactions and community assembly at microscales. *Curr. Opin. Microbiol.* **31**, 227–234 (2016).
4. D'Souza, G. *et al.* Ecology and evolution of metabolic cross-feeding interactions in bacteria. *Nat. Prod. Rep.* **35**, 455–488 (2018).
5. Pierce, E. C. & Dutton, R. J. Putting microbial interactions back into community contexts. *Curr. Opin. Microbiol.* **65**, 56–63 (2022).
6. Kerr, B., Riley, M. A., Feldman, M. W. & Bohannan, B. J. M. Local dispersal promotes biodiversity in a real-life game of rock–paper–scissors. *Nature* **418**, 171–174 (2002).
7. Kirkup, B. C. & Riley, M. A. Antibiotic-mediated antagonism leads to a bacterial game of rock–paper–scissors in vivo. *Nature* **428**, 412–414 (2004).
8. Ghoul, M. & Mitri, S. The Ecology and Evolution of Microbial Competition. *Trends Microbiol.* **24**, 833–845 (2016).
9. García-Bayona, L. & Comstock, L. E. Bacterial antagonism in host-associated microbial communities. *Science* **361**, (2018).
10. Hibbing, M. E., Fuqua, C., Parsek, M. R. & Peterson, S. B. Bacterial competition: surviving and thriving in the microbial jungle. *Nat. Rev. Microbiol.* **8**, 15–25 (2010).
11. Freilich, S. *et al.* Competitive and cooperative metabolic interactions in bacterial

communities. *Nat. Commun.* **2**, 589 (2011).

12. Ghosh, S., Chowdhury, R. & Bhattacharya, P. Mixed consortia in bioprocesses: role of microbial interactions. *Appl. Microbiol. Biotechnol.* **100**, 4283–4295 (2016).
13. Wintermute, E. H. & Silver, P. A. Dynamics in the mixed microbial concourse. *Genes Dev.* **24**, 2603–2614 (2010).
14. Johnson, D. R., Goldschmidt, F., Lilja, E. E. & Ackermann, M. Metabolic specialization and the assembly of microbial communities. *ISME J.* **6**, 1985–1991 (2012).
15. Pande, S. *et al.* Fitness and stability of obligate cross-feeding interactions that emerge upon gene loss in bacteria. *ISME J.* **8**, 953–962 (2013).
16. Germerodt, S. *et al.* Pervasive Selection for Cooperative Cross-Feeding in Bacterial Communities. *PLoS Comput. Biol.* **12**, e1004986 (2016).
17. West, S. A. & Cooper, G. A. Division of labour in microorganisms: an evolutionary perspective. *Nat. Rev. Microbiol.* **14**, 716–723 (2016).
18. Zhang, Z., Claessen, D. & Rozen, D. E. Understanding Microbial Divisions of Labor. *Front. Microbiol.* **7**, 2070 (2016).
19. Tsoi, R. *et al.* Metabolic division of labor in microbial systems. *Proceedings of the National Academy of Sciences* **115**, 2526–2531 (2018).
20. Momeni, B. Division of Labor: How Microbes Split Their Responsibility. *Current biology: CB* vol. 28 R697–R699 (2018).
21. Giri, S., Waschina, S., Kaleta, C. & Kost, C. Defining Division of Labor in Microbial Communities. *J. Mol. Biol.* **431**, 4712–4731 (2019).
22. Rossetti, V., Schirrmeister, B. E., Bernasconi, M. V. & Bagheri, H. C. The evolutionary path to terminal differentiation and division of labor in cyanobacteria. *J. Theor. Biol.* **262**, 23–34 (2010).

23. Roell, G. W. *et al.* Engineering microbial consortia by division of labor. *Microb. Cell Fact.* **18**, 35 (2019).

24. Smith, C. R., Toth, A. L., Suarez, A. V. & Robinson, G. E. Genetic and genomic analyses of the division of labour in insect societies. *Nat. Rev. Genet.* **9**, 735–748 (2008).

25. Gordon, D. M. From division of labor to the collective behavior of social insects. *Behav. Ecol. Sociobiol.* **70**, 1101–1108 (2016).

26. Kirk, D. L. Seeking the ultimate and proximate causes of volvox multicellularity and cellular differentiation. *Integr. Comp. Biol.* **43**, 247–253 (2003).

27. Kirk, D. L. A twelve-step program for evolving multicellularity and a division of labor. *Bioessays* **27**, 299–310 (2005).

28. Costa, E., Pérez, J. & Kreft, J.-U. Why is metabolic labour divided in nitrification? *Trends Microbiol.* **14**, 213–219 (2006).

29. Schmidt, E. L. Nitrification in Soil. in *Nitrogen in Agricultural Soils* 253–288 (American Society of Agronomy, Crop Science Society of America, Soil Science Society of America, 2015).

30. Schink, B. & Pfennig, N. Fermentation of trihydroxybenzenes by Pelobacter acidigallici gen. nov. sp. nov., a new strictly anaerobic, non-sporeforming bacterium. *Arch. Microbiol.* **133**, 195–201 (1982).

31. Shou, W., Ram, S. & Vilar, J. M. G. Synthetic cooperation in engineered yeast populations. *Proceedings of the National Academy of Sciences* **104**, 1877–1882 (2007).

32. Goyal, G., Tsai, S.-L., Madan, B., DaSilva, N. A. & Chen, W. Simultaneous cell growth and ethanol production from cellulose by an engineered yeast consortium displaying a functional mini-cellulosome. *Microb. Cell Fact.* **10**, 89 (2011).

33. Argyros D. Aaron *et al.* High Ethanol Titers from Cellulose by Using Metabolically

Engineered Thermophilic, Anaerobic Microbes. *Appl. Environ. Microbiol.* **77**, 8288–8294 (2011).

34. Xia, T., Eiteman, M. A. & Altman, E. Simultaneous utilization of glucose, xylose and arabinose in the presence of acetate by a consortium of Escherichia coli strains. *Microb. Cell Fact.* **11**, 77 (2012).
35. Zuroff, T. R., Xiques, S. B. & Curtis, W. R. Consortia-mediated bioprocessing of cellulose to ethanol with a symbiotic Clostridium phytofermentans/yeast co-culture. *Biotechnol. Biofuels* **6**, 59 (2013).
36. Trinh Cong T., Unrean Pornkamol & Srienc Friedrich. Minimal Escherichia coli Cell for the Most Efficient Production of Ethanol from Hexoses and Pentoses. *Appl. Environ. Microbiol.* **74**, 3634–3643 (2008).
37. Bokinsky, G. *et al.* Synthesis of three advanced biofuels from ionic liquid-pretreated switchgrass using engineered Escherichia coli. *Proc. Natl. Acad. Sci. U. S. A.* **108**, 19949–19954 (2011).
38. Den Haan, R., Rose, S. H., Lynd, L. R. & van Zyl, W. H. Hydrolysis and fermentation of amorphous cellulose by recombinant Saccharomyces cerevisiae. *Metab. Eng.* **9**, 87–94 (2007).
39. Olson, D. G., McBride, J. E., Shaw, A. J. & Lynd, L. R. Recent progress in consolidated bioprocessing. *Curr. Opin. Biotechnol.* **23**, 396–405 (2012).
40. Minty, J. J. *et al.* Design and characterization of synthetic fungal-bacterial consortia for direct production of isobutanol from cellulosic biomass. *Proceedings of the National Academy of Sciences* **110**, 14592–14597 (2013).
41. Atkinson, E., Tuza, Z., Perrino, G., Stan, G.-B. & Ledesma-Amaro, R. Resource-aware whole-cell model of division of labour in a microbial consortium for complex-substrate

degradation. *Microb. Cell Fact.* **21**, 115 (2022).

42. Pande, S. *et al.* Privatization of cooperative benefits stabilizes mutualistic cross-feeding interactions in spatially structured environments. *ISME J.* **10**, 1413–1423 (2015).
43. Du, J., Shao, Z. & Zhao, H. Engineering microbial factories for synthesis of value-added products. *J. Ind. Microbiol. Biotechnol.* **38**, 873–890 (2011).
44. Jawed, K., Yazdani, S. S. & Koffas, M. A. G. Advances in the development and application of microbial consortia for metabolic engineering. *Metabolic Engineering Communications* **9**, e00095 (2019).
45. Guan, Y. *et al.* Mitigating Host Burden of Genetic Circuits by Engineering Autonegatively Regulated Parts and Improving Functional Prediction. *ACS Synth. Biol.* **11**, 2361–2371 (2022).
46. Weber, C. *et al.* Biosynthesis of cis,cis-muconic acid and its aromatic precursors, catechol and protocatechuic acid, from renewable feedstocks by Saccharomyces cerevisiae. *Appl. Environ. Microbiol.* **78**, 8421–8430 (2012).
47. Zhang, H., Li, Z., Pereira, B. & Stephanopoulos, G. Engineering E. coli-E. coli cocultures for production of muconic acid from glycerol. *Microb. Cell Fact.* **14**, 134 (2015).
48. Zhang, H., Pereira, B., Li, Z. & Stephanopoulos, G. Engineering *Escherichia coli* coculture systems for the production of biochemical products. *Proceedings of the National Academy of Sciences* **112**, 8266–8271 (2015).
49. Zhang, H. & Stephanopoulos, G. Co-culture engineering for microbial biosynthesis of 3-amino-benzoic acid in Escherichia coli. *Biotechnol. J.* **11**, 981–987 (2016).
50. Lindemann, S. R. *et al.* Engineering microbial consortia for controllable outputs. *ISME J.* **10**, 2077–2084 (2016).
51. Chen, T. *et al.* Development and optimization of a microbial co-culture system for

heterologous indigo biosynthesis. *Microb. Cell Fact.* **20**, 154 (2021).

52. Zhou, K., Qiao, K., Edgar, S. & Stephanopoulos, G. Distributing a metabolic pathway among a microbial consortium enhances production of natural products. *Nat. Biotechnol.* **33**, 377–383 (2015).
53. Wang, X., Policarpio, L., Prajapati, D., Li, Z. & Zhang, H. Developing E. coli-E. coli co-cultures to overcome barriers of heterologous tryptamine biosynthesis. *Metabolic Engineering Communications* **10**, e00110 (2020).
54. Draths, K. M. & Frost, J. W. Environmentally compatible synthesis of adipic acid from D-glucose. *J. Am. Chem. Soc.* **116**, 399–400 (1994).
55. Park, J. *et al.* Molecular Time Sharing through Dynamic Pulsing in Single Cells. *cels* **6**, 216-229.e15 (2018).
56. Rosenthal, A. Z. *et al.* Metabolic interactions between dynamic bacterial subpopulations. *Elife* **7**, (2018).
57. Flores, E. & Herrero, A. Compartmentalized function through cell differentiation in filamentous cyanobacteria. *Nat. Rev. Microbiol.* **8**, 39–50 (2009).
58. Stal, L. J. & Krumbein, W. E. Temporal separation of nitrogen fixation and photosynthesis in the filamentous, non-heterocystous cyanobacterium Oscillatoria sp. *Arch. Microbiol.* **149**, 76–80 (1987).
59. Gaudana, S. B. *et al.* Rhythmic and sustained oscillations in metabolism and gene expression of Cyanothece sp. ATCC 51142 under constant light. *Front. Microbiol.* **4**, 374 (2013).
60. Cohen, S. E. & Golden, S. S. Circadian Rhythms in Cyanobacteria. *Microbiol. Mol. Biol. Rev.* **79**, 373–385 (2015).
61. Elowitz, M. B., Levine, A. J., Siggia, E. D. & Swain, P. S. Stochastic Gene Expression in a Single Cell. *Science* **297**, 1183–1186 (2002).

62. Paulsson, J. Models of stochastic gene expression. *Phys. Life Rev.* **2**, 157–175 (2005).

63. Raj, A. & van Oudenaarden, A. Nature, Nurture, or Chance: Stochastic Gene Expression and Its Consequences. *Cell* **135**, 216–226 (2008).

64. Sampaio, N. M. V., Blassick, C. M., Andreani, V., Lugagne, J.-B. & Dunlop, M. J. Dynamic gene expression and growth underlie cell-to-cell heterogeneity in *Escherichia coli* stress response. *Proceedings of the National Academy of Sciences* **119**, e2115032119 (2022).

65. McCallum, G. & Potvin-Trottier, L. Using Models to (Re-)Design Synthetic Circuits. *Methods Mol. Biol.* **2229**, 91–118 (2021).

66. Gardner, T. S., Cantor, C. R. & Collins, J. J. Construction of a genetic toggle switch in Escherichia coli. *Nature* **403**, 339–342 (2000).

67. Potvin-Trottier, L., Lord, N. D., Vinnicombe, G. & Paulsson, J. Synchronous long-term oscillations in a synthetic gene circuit. *Nature* **538**, 514–517 (2016).

68. Larson, M. H. *et al.* CRISPR interference (CRISPRi) for sequence-specific control of gene expression. *Nat. Protoc.* **8**, 2180–2196 (2013).

69. Elowitz, M. B. & Leibler, S. A synthetic oscillatory network of transcriptional regulators. *Nature* **403**, 335–338 (2000).

70. Liao, C. *et al.* Modular one-pot assembly of CRISPR arrays enables library generation and reveals factors influencing crRNA biogenesis. *Nat. Commun.* **10**, 1–14 (2019).

71. Zhang, X. *et al.* Multiplex gene regulation by CRISPR-ddCpf1. *Cell Discovery* **3**, 1–9 (2017).

72. Meliawati, M., Schilling, C. & Schmid, J. Recent advances of Cas12a applications in bacteria. *Appl. Microbiol. Biotechnol.* **105**, 2981–2990 (2021).

73. Miao, C., Zhao, H., Qian, L. & Lou, C. Systematically investigating the key features of the DNase deactivated Cpf1 for tunable transcription regulation in prokaryotic cells. *Synthetic*

and Systems Biotechnology **4**, 1–9 (2019).

74. Hawkins, J. S., Wong, S., Peters, J. M., Almeida, R. & Qi, L. S. Targeted Transcriptional Repression in Bacteria Using CRISPR Interference (CRISPRi). *Methods Mol. Biol.* **1311**, 349–362 (2015).
75. Vigouroux, A., Oldewurtel, E., Cui, L., Bikard, D. & van Teeffelen, S. Tuning dCas9's ability to block transcription enables robust, noiseless knockdown of bacterial genes. *Mol. Syst. Biol.* **14**, e7899 (2018).
76. Fontana, J., Dong, C., Ham, J. Y., Zalatan, J. G. & Carothers, J. M. Regulated Expression of sgRNAs Tunes CRISPRi in E. coli. *Biotechnol. J.* **13**, e1800069 (2018).
77. Rousset, F. *et al.* Genome-wide CRISPR-dCas9 screens in E. coli identify essential genes and phage host factors. *PLoS Genet.* **14**, e1007749 (2018).
78. Depardieu, F. & Bikard, D. Gene silencing with CRISPRi in bacteria and optimization of dCas9 expression levels. *Methods* **172**, 61–75 (2020).
79. Cui, L. *et al.* A CRISPRi screen in E. coli reveals sequence-specific toxicity of dCas9. *Nat. Commun.* **9**, 1–10 (2018).
80. Zhang, S. & Voigt, C. A. Engineered dCas9 with reduced toxicity in bacteria: implications for genetic circuit design. *Nucleic Acids Res.* **46**, 11115–11125 (2018).
81. Deltcheva, E. *et al.* CRISPR RNA maturation by trans-encoded small RNA and host factor RNase III. *Nature* **471**, 602–607 (2011).
82. Wang, P. *et al.* Robust growth of Escherichia coli. *Curr. Biol.* **20**, 1099–1103 (2010).
83. Arnaouteli, S., Bamford, N. C., Stanley-Wall, N. R. & Kovács, Á. T. Bacillus subtilis biofilm formation and social interactions. *Nat. Rev. Microbiol.* **19**, 600–614 (2021).
84. Dar, D., Dar, N., Cai, L. & Newman, D. K. Spatial transcriptomics of planktonic and sessile bacterial populations at single-cell resolution. *Science* **373**, eabi4882 (2021).

85. Veening, J.-W., Smits, W. K. & Kuipers, O. P. Bistability, Epigenetics, and Bet-Hedging in Bacteria. *Annu. Rev. Microbiol.* **62**, 193–210 (2008).

86. Morawska, L. P., Hernandez-Valdes, J. A. & Kuipers, O. P. Diversity of bet-hedging strategies in microbial communities-Recent cases and insights. *WIREs Mech Dis* **14**, e1544 (2022).

87. Karaayvaz, M. *et al.* Unravelling subclonal heterogeneity and aggressive disease states in TNBC through single-cell RNA-seq. *Nat. Commun.* **9**, 3588 (2018).

88. Kinker, G. S. *et al.* Pan-cancer single-cell RNA-seq identifies recurring programs of cellular heterogeneity. *Nat. Genet.* **52**, 1208–1218 (2020).

89. Peyrusson, F. *et al.* Intracellular Staphylococcus aureus persisters upon antibiotic exposure. *Nat. Commun.* **11**, 2200 (2020).

90. Young, J. W. *et al.* Measuring single-cell gene expression dynamics in bacteria using fluorescence time-lapse microscopy. *Nat. Protoc.* **7**, 80–88 (2011).

91. Moffitt, J. R., Lee, J. B. & Cluzel, P. The single-cell chemostat: an agarose-based, microfluidic device for high-throughput, single-cell studies of bacteria and bacterial communities. *Lab Chip* **12**, 1487–1494 (2012).

92. Hardo, G. & Bakshi, S. Challenges of analysing stochastic gene expression in bacteria using single-cell time-lapse experiments. *Essays Biochem.* **65**, 67–79 (2021).

93. Balaban, N. Q., Merrin, J., Chait, R., Kowalik, L. & Leibler, S. Bacterial persistence as a phenotypic switch. *Science* **305**, 1622–1625 (2004).

94. Cookson, S., Ostroff, N., Pang, W. L., Volfson, D. & Hasty, J. Monitoring dynamics of single-cell gene expression over multiple cell cycles. *Mol. Syst. Biol.* **1**, 2005.0024 (2005).

95. Ullman, G. *et al.* High-throughput gene expression analysis at the level of single proteins using a microfluidic turbidostat and automated cell tracking. *Philos. Trans. R. Soc. Lond. B*

Biol. Sci. **368**, 20120025 (2013).

96. Danino, T., Mondragón-Palomino, O., Tsimring, L. & Hasty, J. A synchronized quorum of genetic clocks. *Nature* **463**, 326–330 (2010).
97. Prindle, A. *et al.* A sensing array of radically coupled genetic 'biopixels.' *Nature* **481**, 39–44 (2011).
98. Din, M. O. *et al.* Synchronized cycles of bacterial lysis for in vivo delivery. *Nature* **536**, 81–85 (2016).
99. Scott, S. R. & Hasty, J. Quorum Sensing Communication Modules for Microbial Consortia. *ACS Synth. Biol.* **5**, 969–977 (2016).
100. Miano, A., Liao, M. J. & Hasty, J. Inducible cell-to-cell signaling for tunable dynamics in microbial communities. *Nat. Commun.* **11**, 1–8 (2020).
101. Balleza, E., Kim, J. M. & Cluzel, P. Systematic characterization of maturation time of fluorescent proteins in living cells. *Nat. Methods* **15**, 47–51 (2017).
102. Weibel, D. B., Diluzio, W. R. & Whitesides, G. M. Microfabrication meets microbiology. *Nat. Rev. Microbiol.* **5**, 209–218 (2007).
103. Hol, F. J. H. & Dekker, C. Zooming in to see the bigger picture: microfluidic and nanofabrication tools to study bacteria. *Science* **346**, 1251821 (2014).
104. Eland, L. E., Wipat, A., Lee, S., Park, S. & Wu, L. J. Chapter 3 - Microfluidics for bacterial imaging. in *Methods in Microbiology* (eds. Harwood, C. & Jensen, G. J.) vol. 43 69–111 (Academic Press, 2016).
105. Yang, Y., Song, X. & Lindner, A. B. Chapter 2 - Time-lapse microscopy and image analysis of Escherichia coli cells in mother machines. in *Methods in Microbiology* (eds. Harwood, C. & Jensen, G. J.) vol. 43 49–68 (Academic Press, 2016).
106. Bennett, M. R. & Hasty, J. Microfluidic devices for measuring gene network dynamics in

single cells. *Nat. Rev. Genet.* **10**, 628–638 (2009).

107. Wessel, A. K., Hmelo, L., Parsek, M. R. & Whiteley, M. Going local: technologies for exploring bacterial microenvironments. *Nat. Rev. Microbiol.* **11**, 337–348 (2013).

108. Vasdekis, A. E. & Stephanopoulos, G. Review of methods to probe single cell metabolism and bioenergetics. *Metab. Eng.* **27**, 115–135 (2015).

109. Potvin-Trottier, L., Luro, S. & Paulsson, J. Microfluidics and single-cell microscopy to study stochastic processes in bacteria. *Curr. Opin. Microbiol.* **43**, 186–192 (2018).

110. Scheler, O., Postek, W. & Garstecki, P. Recent developments of microfluidics as a tool for biotechnology and microbiology. *Curr. Opin. Biotechnol.* **55**, 60–67 (2019).

111. Yang, D., Jennings, A. D., Borrego, E., Retterer, S. T. & Männik, J. Analysis of Factors Limiting Bacterial Growth in PDMS Mother Machine Devices. *Front. Microbiol.* **9**, 871 (2018).

112. Kaiser, M. *et al.* Monitoring single-cell gene regulation under dynamically controllable conditions with integrated microfluidics and software. *Nat. Commun.* **9**, 212 (2018).

113. Kamande, J. W., Wang, Y. & Taylor, A. M. Cloning SU8 silicon masters using epoxy resins to increase feature replicability and production for cell culture devices. *Biomicrofluidics* **9**, 036502 (2015).

114. Cabeen, M. T. & Losick, R. Single-cell Microfluidic Analysis of Bacillus subtilis. *J. Vis. Exp.* (2018) doi:10.3791/56901.

115. Paintdakhi, A. *et al.* Oufti: an integrated software package for high-accuracy, high-throughput quantitative microscopy analysis. *Mol. Microbiol.* **99**, 767–777 (2016).

116. Sachs, C. C. *et al.* Image-Based Single Cell Profiling: High-Throughput Processing of Mother Machine Experiments. *PLoS One* **11**, e0163453 (2016).

117. Ollion, J., Elez, M. & Robert, L. High-throughput detection and tracking of cells and

intracellular spots in mother machine experiments. *Nat. Protoc.* **14**, 3144–3161 (2019).

118. Smith, A., Metz, J. & Pagliara, S. MMHelper: An automated framework for the analysis of microscopy images acquired with the mother machine. *Sci. Rep.* **9**, 10123 (2019).

119. Lugagne, J.-B., Lin, H. & Dunlop, M. J. DeLTA: Automated cell segmentation, tracking, and lineage reconstruction using deep learning. *PLoS Comput. Biol.* **16**, e1007673 (2020).

120. Ronneberger, O., Fischer, P. & Brox, T. U-Net: Convolutional Networks for Biomedical Image Segmentation. in *Medical Image Computing and Computer-Assisted Intervention – MICCAI 2015* 234–241 (Springer International Publishing, 2015).

121. Ollion, J. & Ollion, C. DistNet: Deep Tracking by Displacement Regression: Application to Bacteria Growing in the Mother Machine. in *Medical Image Computing and Computer Assisted Intervention – MICCAI 2020: 23rd International Conference, Lima, Peru, October 4–8, 2020, Proceedings, Part V* 215–225 (Springer-Verlag, 2020).

122. Julou, T., Zweifel, L., Blank, D., Fiori, A. & van Nimwegen, E. Subpopulations of sensorless bacteria drive fitness in fluctuating environments. *PLoS Biol.* **18**, e3000952 (2020).

123. Bakshi, S. *et al.* Tracking bacterial lineages in complex and dynamic environments with applications for growth control and persistence. *Nat Microbiol* **6**, 783–791 (2021).

124. Lawson, M. J. *et al.* In situ genotyping of a pooled strain library after characterizing complex phenotypes. *Mol. Syst. Biol.* **13**, 947 (2017).

125. Camsund, D. *et al.* Time-resolved imaging-based CRISPRi screening. *Nat. Methods* **17**, 86–92 (2020).

126. Luro, S., Potvin-Trottier, L., Okumus, B. & Paulsson, J. Isolating live cells after high-throughput, long-term, time-lapse microscopy. *Nat. Methods* **17**, 93–100 (2020).

127. Norman, T. M., Lord, N. D., Paulsson, J. & Losick, R. Memory and modularity in cell-fate

decision making. *Nature* **503**, 481–486 (2013).

128. Darnell, C. L. *et al.* The Ribbon-Helix-Helix Domain Protein CdrS Regulates the Tubulin Homolog ftsZ2 To Control Cell Division in Archaea. *MBio* **11**, (2020).

129. Nakaoka, H. & Wakamoto, Y. Aging, mortality, and the fast growth trade-off of Schizosaccharomyces pombe. *PLoS Biol.* **15**, e2001109 (2017).

130. Li, Y. *et al.* Multigenerational silencing dynamics control cell aging. *Proc. Natl. Acad. Sci. U. S. A.* **114**, 11253–11258 (2017).

131. Ryley, J. & Pereira-Smith, O. M. Microfluidics device for single cell gene expression analysis in Saccharomyces cerevisiae. *Yeast* **23**, 1065–1073 (2006).

132. Crane, M. M., Clark, I. B. N., Bakker, E., Smith, S. & Swain, P. S. A microfluidic system for studying ageing and dynamic single-cell responses in budding yeast. *PLoS One* **9**, e100042 (2014).

133. Jo, M. C., Liu, W., Gu, L., Dang, W. & Qin, L. High-throughput analysis of yeast replicative aging using a microfluidic system. *Proc. Natl. Acad. Sci. U. S. A.* **112**, 9364–9369 (2015).

134. Durán, D. C. *et al.* Slipstreaming Mother Machine: A Microfluidic Device for Single-Cell Dynamic Imaging of Yeast. *Micromachines (Basel)* **12**, (2020).

135. Lee, S. S., Avalos Vizcarra, I., Huberts, D. H. E. W., Lee, L. P. & Heinemann, M. Whole lifespan microscopic observation of budding yeast aging through a microfluidic dissection platform. *Proc. Natl. Acad. Sci. U. S. A.* **109**, 4916–4920 (2012).

136. Xie, Z. *et al.* Molecular phenotyping of aging in single yeast cells using a novel microfluidic device. *Aging Cell* **11**, 599–606 (2012).

137. Zhang, Y. *et al.* Single cell analysis of yeast replicative aging using a new generation of microfluidic device. *PLoS One* **7**, e48275 (2012).

138. Angert, E. R. Alternatives to binary fission in bacteria. *Nat. Rev. Microbiol.* **3**, 214–224

(2005).

139. Facchetti, G., Chang, F. & Howard, M. Controlling cell size through sizer mechanisms. *Curr Opin Syst Biol* **5**, 86–92 (2017).

140. Voorn, W. J. & Koppes, L. J. Skew or third moment of bacterial generation times. *Arch. Microbiol.* **169**, 43–51 (1998).

141. Amir, A. Cell Size Regulation in Bacteria. *Phys. Rev. Lett.* **112**, 208102 (2014).

142. Campos, M. *et al.* A constant size extension drives bacterial cell size homeostasis. *Cell* **159**, 1433–1446 (2014).

143. Wallden, M., Fange, D., Lundius, E. G., Baltekin, Ö. & Elf, J. The Synchronization of Replication and Division Cycles in Individual E. coli Cells. *Cell* **166**, 729–739 (2016).

144. Taheri-Araghi, S. *et al.* Cell-size control and homeostasis in bacteria. *Curr. Biol.* **25**, 385–391 (2015).

145. Sauls, J. T. *et al.* Control of Bacillus subtilis Replication Initiation during Physiological Transitions and Perturbations. *MBio* **10**, (2019).

146. Si, F. *et al.* Mechanistic Origin of Cell-Size Control and Homeostasis in Bacteria. *Curr. Biol.* **29**, 1760-1770.e7 (2019).

147. Witz, G., van Nimwegen, E. & Julou, T. Initiation of chromosome replication controls both division and replication cycles in E. coli through a double-adder mechanism. *Elife* **8**, (2019).

148. Nieto, C., Arias-Castro, J., Sánchez, C., Vargas-García, C. & Pedraza, J. M. Unification of cell division control strategies through continuous rate models. *Phys Rev E* **101**, 022401 (2020).

149. Ho, P.-Y. & Amir, A. Simultaneous regulation of cell size and chromosome replication in bacteria. *Front. Microbiol.* **6**, 662 (2015).

150. Micali, G., Grilli, J., Osella, M. & Lagomarsino, M. C. Concurrent processes set *E. coli* cell

division. *Science Advances* **4**, eaau3324 (2018).

151. Le Treut, G., Si, F., Li, D. & Jun, S. Quantitative Examination of Five Stochastic Cell-Cycle and Cell-Size Control Models for Escherichia coli and Bacillus subtilis. *Front. Microbiol.* **12**, 721899 (2021).

152. Gordo, I., Perfeito, L. & Sousa, A. Fitness effects of mutations in bacteria. *J. Mol. Microbiol. Biotechnol.* **21**, 20–35 (2011).

153. Tomanek, I. *et al.* Gene amplification as a form of population-level gene expression regulation. *Nat Ecol Evol* **4**, 612–625 (2020).

154. Robert, L. *et al.* Mutation dynamics and fitness effects followed in single cells. *Science* **359**, 1283–1286 (2018).

155. Robert, L., Ollion, J. & Elez, M. Real-time visualization of mutations and their fitness effects in single bacteria. *Nat. Protoc.* **14**, 3126–3143 (2019).

156. Wiktor, J. *et al.* RecA finds homologous DNA by reduced dimensionality search. *Nature* **597**, 426–429 (2021).

157. Uphoff, S. *et al.* Stochastic activation of a DNA damage response causes cell-to-cell mutation rate variation. *Science* **351**, 1094–1097 (2016).

158. Uphoff, S. Real-time dynamics of mutagenesis reveal the chronology of DNA repair and damage tolerance responses in single cells. *Proc. Natl. Acad. Sci. U. S. A.* **115**, E6516–E6525 (2018).

159. Vincent, M. S. & Uphoff, S. Cellular heterogeneity in DNA alkylation repair increases population genetic plasticity. *Nucleic Acids Res.* **49**, 12320–12331 (2021).

160. Moger-Reischer, R. Z. & Lennon, J. T. Publisher Correction: Microbial ageing and longevity. *Nat. Rev. Microbiol.* **17**, 716 (2019).

161. Knorre, D. A., Azbarova, A. V., Galkina, K. V., Feniouk, B. A. & Severin, F. F. Replicative

aging as a source of cell heterogeneity in budding yeast. *Mech. Ageing Dev.* **176**, 24–31 (2018).

162. Proenca, A. M., Rang, C. U., Buetz, C., Shi, C. & Chao, L. Age structure landscapes emerge from the equilibrium between aging and rejuvenation in bacterial populations. *Nat. Commun.* **9**, 3722 (2018).

163. Bergmiller, T. *et al.* Biased partitioning of the multidrug efflux pump AcrAB-TolC underlies long-lived phenotypic heterogeneity. *Science* **356**, 311–315 (2017).

164. Mäkelä, J., Uphoff, S. & Sherratt, D. J. Nonrandom segregation of sister chromosomes by *Escherichia coli* MukBEF. *Proceedings of the National Academy of Sciences* **118**, e2022078118 (2021).

165. Lindner, A. B., Madden, R., Demarez, A., Stewart, E. J. & Taddei, F. Asymmetric segregation of protein aggregates is associated with cellular aging and rejuvenation. *Proc. Natl. Acad. Sci. U. S. A.* **105**, 3076–3081 (2008).

166. Proenca, A. M., Rang, C. U., Qiu, A., Shi, C. & Chao, L. Cell aging preserves cellular immortality in the presence of lethal levels of damage. *PLoS Biol.* **17**, e3000266 (2019).

167. Łapińska, U., Glover, G., Capilla-Lasheras, P., Young, A. J. & Pagliara, S. Bacterial ageing in the absence of external stressors. *Philos. Trans. R. Soc. Lond. B Biol. Sci.* **374**, 20180442 (2019).

168. Landgraf, D., Okumus, B., Chien, P., Baker, T. A. & Paulsson, J. Segregation of molecules at cell division reveals native protein localization. *Nat. Methods* **9**, 480–482 (2012).

169. Govers, S. K., Mortier, J., Adam, A. & Aertsen, A. Protein aggregates encode epigenetic memory of stressful encounters in individual Escherichia coli cells. *PLoS Biol.* **16**, e2003853 (2018).

170. Kim, J. M., Garcia-Alcala, M., Balleza, E. & Cluzel, P. Stochastic transcriptional pulses

orchestrate flagellar biosynthesis in *Escherichia coli*. *Science Advances* **6**, eaax0947 (2020).

171. Patange, O. *et al.* Escherichia coli can survive stress by noisy growth modulation. *Nat. Commun.* **9**, 5333 (2018).

172. Locke, J. C. W., Young, J. W., Fontes, M., Hernández Jiménez, M. J. & Elowitz, M. B. Stochastic pulse regulation in bacterial stress response. *Science* **334**, 366–369 (2011).

173. Jones, E. C. & Uphoff, S. Single-molecule imaging of LexA degradation in Escherichia coli elucidates regulatory mechanisms and heterogeneity of the SOS response. *Nat Microbiol* **6**, 981–990 (2021).

174. Cabeen, M. T., Russell, J. R., Paulsson, J. & Losick, R. Use of a microfluidic platform to uncover basic features of energy and environmental stress responses in individual cells of Bacillus subtilis. *PLoS Genet.* **13**, e1006901 (2017).

175. Schwall, C. P. *et al.* Tunable phenotypic variability through an autoregulatory alternative sigma factor circuit. *Mol. Syst. Biol.* **17**, e9832 (2021).

176. Lord, N. D. *et al.* Stochastic antagonism between two proteins governs a bacterial cell fate switch. *Science* **366**, 116–120 (2019).

177. Russell, J. R., Cabeen, M. T., Wiggins, P. A., Paulsson, J. & Losick, R. Noise in a phosphorelay drives stochastic entry into sporulation in Bacillus subtilis. *EMBO J.* **36**, 2856–2869 (2017).

178. Aslam, B. *et al.* Antibiotic resistance: a rundown of a global crisis. *Infect. Drug Resist.* **11**, 1645–1658 (2018).

179. Balaban, N. Q. *et al.* Definitions and guidelines for research on antibiotic persistence. *Nat. Rev. Microbiol.* **17**, 441–448 (2019).

180. Goode, O. *et al.* Persister Escherichia coli Cells Have a Lower Intracellular pH than Susceptible Cells but Maintain Their pH in Response to Antibiotic Treatment. *MBio* **12**,

e0090921 (2021).

181. Manuse, S. *et al.* Bacterial persisters are a stochastically formed subpopulation of low-energy cells. *PLoS Biol.* **19**, e3001194 (2021).

182. Goode, O. *et al.* Heterologous Protein Expression Favors the Formation of Protein Aggregates in Persister and Viable but Nonculturable Bacteria. *ACS Infect Dis* **7**, 1848–1858 (2021).

183. Baltekin, Ö., Boucharin, A., Tano, E., Andersson, D. I. & Elf, J. Antibiotic susceptibility testing in less than 30 min using direct single-cell imaging. *Proc. Natl. Acad. Sci. U. S. A.* **114**, 9170–9175 (2017).

184. Cama, J. *et al.* Single-cell microfluidics facilitates the rapid quantification of antibiotic accumulation in Gram-negative bacteria. *Lab Chip* **20**, 2765–2775 (2020).

185. Stricker, J. *et al.* A fast, robust and tunable synthetic gene oscillator. *Nature* **456**, 516–519 (2008).

186. Lezia, A., Csicsery, N. & Hasty, J. Design, mutate, screen: Multiplexed creation and arrayed screening of synchronized genetic clocks. *Cell Syst* **13**, 365-375.e5 (2022).

187. Niederholtmeyer, H. *et al.* Rapid cell-free forward engineering of novel genetic ring oscillators. *Elife* **4**, e09771 (2015).

188. Zhang, F. *et al.* Independent control of amplitude and period in a synthetic oscillator circuit with modified repressilator. *Commun Biol* **5**, 23 (2022).

189. Lugagne, J.-B. *et al.* Balancing a genetic toggle switch by real-time feedback control and periodic forcing. *Nat. Commun.* **8**, 1671 (2017).

190. Cooper, R. M., Tsimring, L. & Hasty, J. Inter-species population dynamics enhance microbial horizontal gene transfer and spread of antibiotic resistance. *Elife* **6**, e25950 (2017).

191. Pearl Mizrahi, S., Gefen, O., Simon, I. & Balaban, N. Q. Persistence to anti-cancer

treatments in the stationary to proliferating transition. *Cell Cycle* **15**, 3442–3453 (2016).

192. Seita, A., Nakaoka, H., Okura, R. & Wakamoto, Y. Intrinsic growth heterogeneity of mouse leukemia cells underlies differential susceptibility to a growth-inhibiting anticancer drug. *PLoS One* **16**, e0236534 (2021).

193. Huang, S. Non-genetic heterogeneity of cells in development: more than just noise. *Development* **136**, 3853–3862 (2009).

194. Jolly, M. K., Kulkarni, P., Weninger, K., Orban, J. & Levine, H. Phenotypic Plasticity, Bet-Hedging, and Androgen Independence in Prostate Cancer: Role of Non-Genetic Heterogeneity. *Front. Oncol.* **8**, 50 (2018).

195. Reyes, J. & Lahav, G. Leveraging and coping with uncertainty in the response of individual cells to therapy. *Curr. Opin. Biotechnol.* **51**, 109–115 (2018).

196. Stuart, T. & Satija, R. Integrative single-cell analysis. *Nat. Rev. Genet.* **20**, 257–272 (2019).

197. Chandrasekaran, S. N., Ceulemans, H., Boyd, J. D. & Carpenter, A. E. Image-based profiling for drug discovery: due for a machine-learning upgrade? *Nat. Rev. Drug Discov.* **20**, 145–159 (2020).

198. Yuan, A. H. & Hochschild, A. A bacterial global regulator forms a prion. *Science* **355**, 198–201 (2017).

199. Fleming, E., Yuan, A. H., Heller, D. M. & Hochschild, A. A bacteria-based genetic assay detects prion formation. *Proc. Natl. Acad. Sci. U. S. A.* **116**, 4605–4610 (2019).

200. Wong, W. W., Tsai, T. Y. & Liao, J. C. Single-cell zeroth-order protein degradation enhances the robustness of synthetic oscillator. *Mol. Syst. Biol.* **3**, 130 (2007).

201. Gefen, O., Fridman, O., Ronin, I. & Balaban, N. Q. Direct observation of single stationary-phase bacteria reveals a surprisingly long period of constant protein production activity. *Proceedings of the National Academy of Sciences* **111**, 556–561 (2014).

202. Siegele, D. A. & Hu, J. C. Gene expression from plasmids containing the *araBAD* promoter at subsaturating inducer concentrations represents mixed populations. *Proceedings of the National Academy of Sciences* **94**, 8168–8172 (1997).

203. Kuo, J., Yuan, R., Sánchez, C., Paulsson, J. & Silver, P. A. Toward a translationally independent RNA-based synthetic oscillator using deactivated CRISPR-Cas. *Nucleic Acids Res.* **48**, 8165–8177 (2020).

204. Moore, S. J. *et al.* EcoFlex: A Multifunctional MoClo Kit for E. coli Synthetic Biology. *ACS Synth. Biol.* **5**, 1059–1069 (2016).

205. Oña, L. *et al.* Obligate cross-feeding expands the metabolic niche of bacteria. *Nature Ecology & Evolution* **5**, 1224–1232 (2021).

206. Riglar, D. T. *et al.* Bacterial variability in the mammalian gut captured by a single-cell synthetic oscillator. *Nat. Commun.* **10**, 1–12 (2019).

207. Santos-Moreno, J., Tasiudi, E., Stelling, J. & Schaerli, Y. Multistable and dynamic CRISPRi-based synthetic circuits. *Nat. Commun.* **11**, 2746 (2020).

208. Miller, J. H. Determination of viable cell counts: Bacterial growth curves. in *Experiments in molecular genetics* (ed. Miller, J. H.) 31–36 (Cold Spring Harbour, 1972).

209. Jones, J. A. *et al.* ePathOptimize: A Combinatorial Approach for Transcriptional Balancing of Metabolic Pathways. *Sci. Rep.* **5**, 11301 (2015).

210. Füller, J. J. *et al.* Biosynthesis of Violacein, Structure and Function of l-Tryptophan Oxidase VioA from Chromobacterium violaceum. *J. Biol. Chem.* **291**, 20068–20084 (2016).

211. Gilbert, L. A. *et al.* CRISPR-Mediated Modular RNA-Guided Regulation of Transcription in Eukaryotes. *Cell* **154**, 442–451 (2013).

212. Cameron, D. E. & Collins, J. J. Tunable protein degradation in bacteria. *Nat. Biotechnol.* **32**, 1276–1281 (2014).

213. Salis, H. M. The ribosome binding site calculator. *Methods Enzymol.* **498**, 19–42 (2011).

214. TerMaat, J. R., Pienaar, E., Whitney, S. E., Mamedov, T. G. & Subramanian, A. Gene synthesis by integrated polymerase chain assembly and PCR amplification using a high-speed thermocycler. *J. Microbiol. Methods* **79**, 295–300 (2009).

215. Labun, K. *et al.* CHOPCHOP v3: expanding the CRISPR web toolbox beyond genome editing. *Nucleic Acids Res.* **47**, W171–W174 (2019).

216. Aoki, S. K. *et al.* A universal biomolecular integral feedback controller for robust perfect adaptation. *Nature* **570**, 533–537 (2019).